

Electronic Supplementary Information For:

Cobalt-Based Molecular Electrocatalysis of Nitrile Reduction: Evolving Sustainability Beyond Hydrogen

Simon N. Child, Radoslav Raychev, Nathan Moss, Benjamin Howchen, Peter N. Horton, Christopher C. Prior, Vasily S. Oganessian and John Fielden*

General

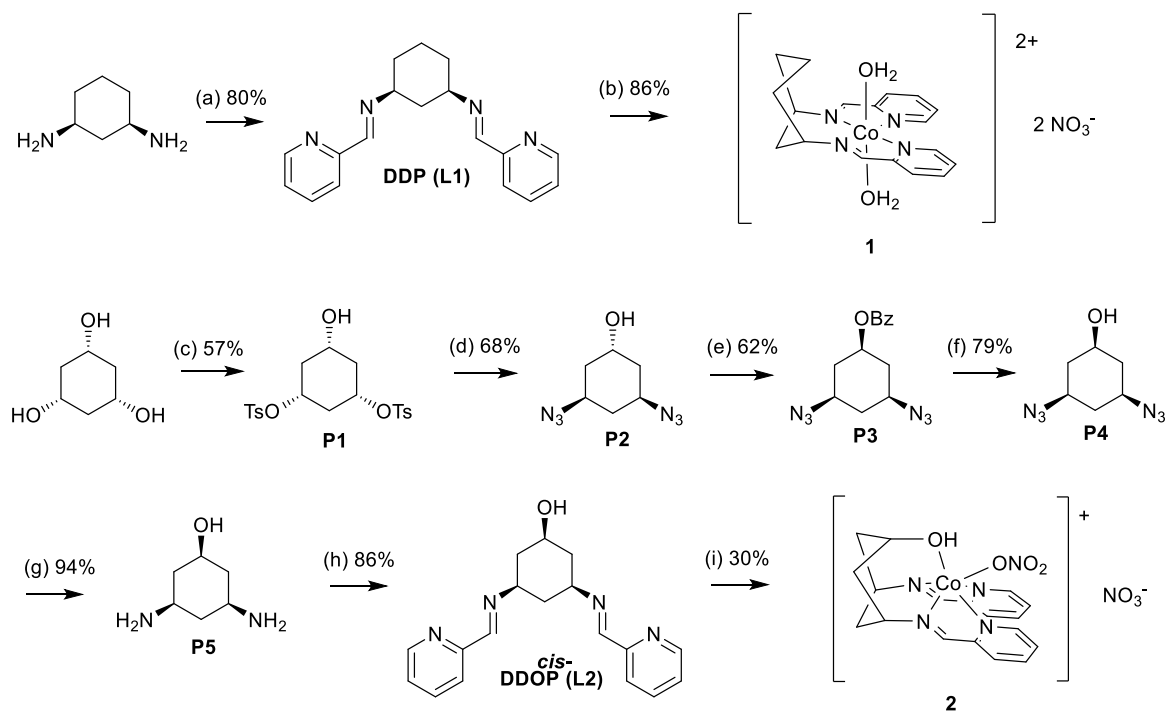
Materials and Procedures. Tetrahydrofuran (THF) was distilled over sodium wire under nitrogen; triethylamine (TEA) was distilled at reduced pressure over KOH and stored over KOH under nitrogen; acetonitrile (MeCN) was distilled over CaH₂ under nitrogen, and dichloromethane was distilled over P₂O₅ and K₂CO₃ under nitrogen.¹ Pyridine was distilled and stored over KOH under nitrogen. Ethanol was dried over 4Å molecular sieves. *cis,cis*-1,3,5-Cyclohexanetriol dihydrate was obtained from Bujno Chemicals (Poland) and dried under high vacuum for 24 hours at 50 °C (until weighing confirmed that all water had been removed). *cis*-1,3-Diaminocyclohexane was obtained from TCI chemicals. All other reagents and solvents were obtained as ACS grade from Sigma-Aldrich, Alfa Aesar or Fisher Scientific and used as supplied. Deuterated solvents were obtained from Goss Scientific. Tosyl chloride (Aldrich) was recrystallised from ethyl acetate after washing with 10% NaOH solution. Unless otherwise stated, all column chromatography was performed over silica gel. Precursor compound **P2** was synthesized following published methods.² *N*-ethyl-2,4-dinitroaniline, *N*-butyl-2,4-dinitroaniline, and *N,N*-dibutyl-2,4-dinitroaniline were all synthesized by reaction of the parent ethyl / butyl amines or their hydrochloride salts with 2,4-dinitrofluorobenzene, according to published methods.³

Physical Measurements. FT-IR spectra were measured using Perkin Elmer FT-IR spectrum BX and Bruker FT-IR XSA spectrometers. ¹H- and ¹³C-NMR spectra were acquired using Bruker AC 300 (300 MHz) and Bruker Ascend 500 (500 MHz) spectrometers and all shifts are quoted with respect to TMS using the solvent signals as secondary standard (s = singlet, d = doublet, t = triplet, q = quartet, sex = sextet, dt = doublet of triplets, m = multiplet). Paramagnetic ¹H NMR spectra for cobalt complexes were recorded using the following parameters; Line broadening (LB) = 2, Acquisition Time (AQ) = 0.5 s, Delay (D₁) = 0.1 s, Sweep Width (SW) = 333.18 ppm, number of scans = 512. Elemental analyses and accurate mass spectrometry were outsourced to London Metropolitan University, and the UK National Mass Spectrometry Service at Swansea University respectively. UV-Vis spectra were obtained by using an Agilent Cary 60 UV-Vis spectrophotometer. Cyclic voltammetry and bulk electrolysis measurements were carried out using Autolab PGStat 30 potentiostat/galvanostat and are described in further detail below. Gas chromatography was performed using a Perkin Elmer Clarus 580 gas chromatograph, controlled using Clarity⁴ software.

Synthetic Methods

Summary: Ligands and Complexes. The Schiff-base ligands **L1** and **L2** were accessed from their precursor amines by a straightforward condensation reaction with 4-pyridine carboxaldehyde. However, the amino-alcohol precursor (**P5**) required for **L2** was obtained by multi-step synthesis starting from *cis*-1,3,5-cyclohexanetriol (Figure S1). This followed a similar approach to that previously used for the *cis*-3,5-diamino-*trans*-hydroxy stereoisomer,² but was shortened by using a direct tosylation of the triol⁵ in place of the previous mono-silylation, tosylation and deprotection. Although this reduces the yield of the ditosylate product **P1** (vs the protection, deprotection strategy), the mono-tosylate by product **P1b** is potentially useful, easily separated and produced in substantial yield. Subsequently, the tosyl groups were displaced by azide to obtain **P2** which undergoes a Mitsunobu inversion,⁶ followed by

hydrolysis, reduction and imination to **L2**. The yield of the Mitsunobu is relatively low, likely because of side reactions between the azide group and PPh₃ which require a low reaction temperature. However, alternative approaches – for example tosylation or triflation of the alcohol group in **3** followed by inversion were ineffective.



Scheme S1 Synthesis of ligands and complexes: (a) 2-pyridinecarboxylaldehyde, NEt₃, MeOH, reflux, 20 h; (b) Co(NO₃)₂•6H₂O, MeOH, 4 h; (c) TsCl, pyridine, 0°C, 18 h (mono-tosylate **2a** 25%); (d) NaN₃, DMF, 70°C, 24 hr; (e) DEAD, PPh₃, BzOH, THF, 3 hr; (f) NaOMe, MeOH, 4 hr; (g) H₂, Pd/C, EtOH, rt, 18 hr; (h) 2-pyridinecarboxylaldehyde, NEt₃, MeOH, reflux, 20 h; (i) Co(NO₃)₂•6H₂O, MeOH, 4 h.

Syntheses

cis-1,3-bis(2-pyridinylenamine] cyclohexane (DDP, L1)

cis-1,3-Diaminocyclohexane (0.88 mmol, 0.122 mL) was added to a solution of 2-pyridinecarboxaldehyde (1.85 mmol, 0.192 mL) and triethylamine (0.44 mmol, 0.06 mL) and refluxed in dry MeOH (60 mL) overnight. The solvent was then removed under reduced pressure and the resultant oil re-dissolved in DCM, which was washed with distilled water and the organic layer dried over MgSO₄. The volume was reduced under vacuum to ca 5 mL then hexane was added and put in the freezer overnight forming **10** as brown crystals (0.2 g, 0.7 mmol, 80%). ¹H-NMR (500 MHz, D₂O): δ 8.06 (dd, 2H, *J* = 5, 2 Hz), 8.46 (s, 2H), 8.04 – 8.02 (m, 2H), 7.9 (*m*, 2H), 7.47 (*m*, 2H), 3.56 (*ptpt*, 2H), 1.97 (*m*, 2H), 1.90 - 1.80 (*m*, 3H), 1.72 – 1.61 (*m*, 3H). ¹³C-NMR (125 MHz, CDCl₃): δ 160.12, 154.82, 149.43, 136.52, 124.62, 121.48, 68.17, 41.31, 33.18, 22.88. FTIR (thin film on CaF₂) cm⁻¹: 1600 (s). *m/z* (ESI⁺): [M+Na] 315.16.

cis-1,3-Ditosyloxy-*trans*-5-hydroxycyclohexane (**2**) and *cis*-1,3-dihydroxy-5-tosyloxycyclohexane (**P1**)

To a vigorously stirred solution of dry *cis,cis*-1,3,5-cyclohexanetriol (0.787 g, 0.596 mmol) in pyridine (13 mL, 16 mmol) at 0 °C was added dropwise a solution of freshly purified and dried tosyl chloride (2.38 g, 1.25 mmol) in pyridine (4 mL, 0.48 mmol) and stirred for 6 hours at 0 °C. The reaction mixture was then allowed to slowly warm to room temperature with stirring overnight. After the reaction was seen to complete by TLC, ethyl acetate (40 mL) was added, and the resulting mixture was washed with (10 mL) of 1 M HCl, followed by water (10 mL), saturated sodium carbonate (10 mL), and brine (10

mL). The organic layer was then dried over sodium sulphate, and the solvent removed to give the crude tosylated compound which was absorbed on the minimum of silica. Flash chromatography with ethyl acetate: hexane (2:1), gave compound **2** as an off white sticky solid (1.503 g, 0.358 mmol, 57%). ¹H-NMR (300 MHz, CDCl₃): δ 7.73 (d, 4H, *J* = 8 Hz), 7.33 (d, 4H, *J* = 8 Hz), 4.32 (m, 2H), 3.53 (m, 1H), 2.44 (s, 6H), 2.23-2.15 (m, 3H), 1.60 (m, 1H), 1.42 (m, 2H). ¹³C-NMR (75 MHz, CDCl₃): δ 145.2 (Ar, C), 133.8 (Ar, C), 130.0 (Ar, CH), 127.6 (Ar, CH), 74.1 (CH), 64.4 (CH), 40.3 (CH₂), 37.7 (CH₂), 21.7 (CH₃). *m/z* (ESI⁺) 441.10 [M+H]⁺. FTIR (thin film on CaF₂) cm⁻¹: 3540 (s), 2958 (m), 2870 (w), 1598 (m), 1495 (w), 1469 (w), 1356 (s), 1173 (s), 1096 (m). Elemental analysis for C₂₆H₃₆O₁₀S₂ calcd (found) %: C 54.63 (54.59), H 5.37 (5.41). Also isolated as the second product from the same column was **P1a** as a white solid (0.04 g, 0.149 mmol, 25%). ¹H-NMR (300 MHz, CDCl₃): δ 7.77 (d, 2H, *J* = 9 Hz), 7.34 (d, 2H, *J* = 9 Hz), 4.47 (m, 1H), 3.68 (m, 2H, H_d), 2.45 (s, 3H), 2.21-2.122 (m, 3H), 1.58 (m, 1H), 1.39 (m, 2H). ¹³C-NMR (75 MHz, CDCl₃): δ 145.0 (Ar, C), 134.3 (Ar, C), 130.0 (Ar,CH), 127.8 (Ar, CH), 75.8 (CH), 65.4 (CH), 42.6 (CH₂), 40.4 (CH₂), 21.8 (CH₃). *m/z* (ESI⁺) 595.16 [2M+Na]⁺. FTIR (thin film on CaF₂) cm⁻¹: 3348 (b), 2947 (sh), 2866 (w), 1597 (m), 1467 (m), 1349 (s), 1189 (s), 1174 (s), 1096 (s), 1024 (s), 953 (s), 928 (s). Elemental analysis for C₁₃H₁₈O₇S, calcd (found) %: C 54.38 (54.53), H 6.37 (6.34).

***cis,cis*-3,5-Diazidocyclohexyl benzoate (P3)**

A solution of *cis*-3,5-diazido-*trans*-hydroxycyclohexane (**3**, 0.56 g, 3.1 mmol) in anhydrous THF (5 mL) was cooled to -50 °C (dry ice/acetone bath) under nitrogen. Benzoic acid (0.62 g, 4.9 mmol) and triphenylphosphine (1.29 g, 4.9 mmol) were then added to the cooled solution in quick succession, followed by the dropwise addition of DEAD (0.86 mL, 4.9 mmol). The reaction mixture was then allowed to warm to room temperature over *ca.* 2 hours and stirred for a further hour at room temperature until completion of the reaction was shown by TLC (hexane: ethyl acetate, 95:5). Ether (10 mL) was added to the reaction mixture, which was then washed with 1 M HCl (10 mL), water (10 mL), saturated sodium bicarbonate solution (10 mL) and brine (10 mL). The ethereal layer was then dried over MgSO₄ and the solvent removed and left overnight for crystals of triphenylphosphine oxide to form. The resulting mixture was taken up in ethyl acetate and evaporated to dryness on silica gel, before purification by column chromatography (hexane: ethyl acetate, 95:5 to 60:40) gave the product **6** as a yellow oil (0.556 g, 62%). ¹H-NMR (500 MHz, CDCl₃): δ 8.02 (dd, *J* = 7.5, 1 Hz, 2H), 7.58 (tt, *J* = 7.5, 1 Hz, 1H), 7.51-7.47 (m, 2H), 5.00 (m, 1H), 3.46 (m, 2H), 2.5-2.44 (m, 2H), 2.37-2.3 (m, 1H), 1.53 (m, 2H), 1.40 (m, 1H). ¹³C-NMR (125 MHz, CDCl₃): δ 165.8 (Ar-COO, C), 133.5 (ArC), 129.86 (ArC), 129.84 (ArC), 128.64 (ArC), 68.4 (CH), 55.1 (CH), 36.8 (CH₂), 36.6 (CH₂). *m/z* (ESI⁺) 259.12 [M-N₂+H]⁺. FTIR (thin film on CaF₂) cm⁻¹: 3324 (w), 2956 (m), 2880 (m), 2506 (w), 2104 (s, sh), 1716 (s, sh), 1604 (m). Elemental analysis for C₁₃H₁₄N₆O₂, calcd (found) %: C 54.54 (54.71), H 4.93 (5.04), N 29.36 (29.46).

***cis*-3,5-Diazido-*cis*-hydroxycyclohexane (P4)**

To a solution of *cis,cis*-3,5-diazidocyclohexyl benzoate (**6**) (100 mg, 0.35 mmol) in anhydrous methanol (2 mL) was added dropwise a solution of sodium methoxide in methanol (0.5 M, 2 mL). After the solution had stirred for 4 hours at room temperature, the solution was washed through Amberlite IR-120 (plus) (prewashed with methanol). Removal of 80% of the solvent and purification by column chromatography (hexane: EtOAc 9:1, then 4:6) yielded **7** as a yellow oil, (50 mg, 79 %). ¹H-NMR (500 MHz, CDCl₃): δ 3.72 (m, 1H), 3.35 (m, 2H), 2.37 – 2.20 (m, 3H), 1.34 (m, 1H), 1.327 (m, 2H). ¹³C-NMR δ (125 MHz, CDCl₃): 66.4 (CH), 55.2 (CH), 40.0 (CH₂), 36.5 (CH₂). *m/z* (ESI⁺) 205.08 [M+Na]⁺. FTIR (thin film on CaF₂) cm⁻¹: 3330 (br), 2926 (s), 2858 (s), 2486 (s), 2094 (sh). Elemental analysis for C₁₃H₁₄N₆O₂, calcd (found) %: C 39.56 (39.80), H 5.53 (5.67), N 46.13 (45.89).

***cis*-3,5-Diamino-*cis*-hydroxycyclohexane (P5)**

10% Pd/C (0.020 g, mmol) was added to a solution of *cis*-3,5-diazo-*cis*-hydroxycyclohexane (**7**) (0.126 g, 0.691 mmol) in ethanol (3.5 mL). This was treated with hydrogen at 620 kPa, at 30 °C with stirring for 18 hours. Removal of Pd/C by filtration, followed by evaporation of the solvent gave the product **8** as a white solid (0.085 g, 0.65 mmol, 94%). ¹H-NMR (500 MHz, D₂O): δ 3.68 (m, 1H), 3.74 (m, 2H), 2.1-2.04 (m, 2H), 1.96 – 1.90 (m, 1H), 1.04 (m, 2H), 0.90 (m, 1H). ¹³C-NMR (125 MHz, D₂O): δ 67.03 (CH), 45.70 (CH), 42.7 (CH₂), 42.41 (CH₂). *m/z* (ESI⁺) 153.09 [M+Na]⁺. FTIR (thin film on CaF₂) cm⁻¹: 3279 (sh), 2929 (sh), 1596 (s), 1554 (s), 1458 (s), 1356 (s), 1284 (s), 1257 (w), 1022 (w), 910 (m).

***cis*-3,5-Bis[(2-pyridinyl)eneamin]-*cis*-hydroxycyclohexane (L2)**

A methanolic solution (5 mL) of 2-pyridinecarboxaldehyde (0.41 g, 3.54 mmol) was added to a solution of *cis*-3,5-diamino-*cis*-hydroxycyclohexane (**8**) (0.230 g, 1.77 mmol) and triethylamine (0.09 g, 0.88 mmol) in methanol (40 mL). The mixture was refluxed under nitrogen for 20 hours and the volume was then reduced to give a brown oil. This was extracted from water with chloroform (3 × 50 mL), the organic layer back-extracted with water (3 × 50 mL) and dried over MgSO₄. The brown oil was then dissolved in the minimum of diethyl ether and precipitated by addition of hexane, filtration and drying under vacuum gave the product **9** (0.481 g, 1.55 mmol, 86%) as a cream solid. ¹H-NMR (500 MHz, CDCl₃): δ 8.65 (dd, 2H, *J* = 5, 2 Hz), 8.44 (s, 2H), 8.02 - 7.99 (m, 2H), 7.74 (*m*, 2H), 7.32 (*m*, 2H), 3.97 (*m*, 1H), 3.55 (*m*, 2H, H), 2.19-2.12 (m, 2H), 1.97 (*pq*, 1H), 1.89-1.81 (m, 1H), 1.74 (*pq*, 2H). ¹³C-NMR (125 MHz, CDCl₃): δ 160.8 (CN-imine), 154.7 (py -CN), 149.6 (py -CN), 136.7 (py -C), 124.9 (py -C), 121.7 (py -C), 65.6 (CH), 42.6 (CH₂), 40.7 (CH₂). *m/z* (ESI⁺) 331.15 [M+Na]⁺. FTIR (thin film on CaF₂) cm⁻¹: 3352 (br, sh), 3059 (w), 3010 (w), 2935 (s), 2860 (s), 2217 (w), 1645 (s), 1588 (s), 1567 (s), 1469 (s), 1436 (s), 1337 (s), 1225 (s), 1086 (s), 1026 (m), 992 (w).

[Co(L1)(H₂O)₂](NO₃)₂ (1**, CoL1)**

L1 (0.021 g, 0.07185 mmol) as a 0.01 M methanolic solution (7 mL) was added dropwise over 3.5 hours to a solution of Co(NO₃)₂·6H₂O (0.022 g, 0.007185 mmol) in methanol (1 mL). A colour change from pink to orange was observed. After the addition was complete the solution was stirred for a further 30 minutes, reduced to *ca* 3 mL and set to crystallise by Et₂O diffusion. After 12 hours orange-brown crystals of **CoL1N** were formed (40 mg, 0.062 mmol, 86%). ¹H-NMR (300 MHz, CD₃OD): δ 73.63 - 77.67, 64.86, 37.61, 22.46, 1.60 - 3.07, 1.51 - 1.98, 0.91 - 1.05, -6.75, -15.99, -16.6, -38.08, -36.36, -50.12, -59.33, -57.14. *m/z* (ESI⁺): 350.09 [M+ -N₂O₆H]. IR (MeOH) /cm⁻¹: 1650 (s). Elemental analysis for C₁₈H₂₀CoN₆O₆ calcd (found) %: C 45.48 (45.30), H 4.24 (4.10), N 17.68 (17.90).

[Co(L2)(NO₃)H₂O](NO₃) (2**, CoL2)**

L3 (20 mg, 0.06 mmol) as a 0.01 M methanolic solution (7 mL) was added dropwise over 3.5 hours to a solution of Co(NO₃)₂·6H₂O (23 mg, 0.06 mmol) in methanol (0.5 mL). A colour change from pink to brown was observed. After the addition was complete the solution was stirred for a further 30 minutes, reduced to *c.a.* 2 mL and set to crystallise by Et₂O diffusion. After 1-week brown crystals of **CoL3N** were grown by Et₂O diffusion (7.8 mg, 0.018 mmol, 30%). ¹H-NMR (300 MHz, CD₃OD): δ 66 (sh), 47, 41, 35 (br), 28 (sh), 23 (br), 7, 5, 1, 0. *m/z* (ESI⁺): 429.08 [M-NO₃]⁺. FTIR (thin film on CaF₂) cm⁻¹: 3096 (m) (OH), 2929 (w) (CH), 1650 (m) 1599 (s) (C=N), 1446 (s), 1391 (s), 1309 (coordinated NO₃⁻), 1128 (m) (C-O). Elemental analysis for C₁₈H₂₀CoN₆O₇, calcd (found) %: C 44.0 (43.56), H 4.10 (4.15), N 17.11 (16.94).

Electrochemistry and Electrocatalysis

Cyclic voltammetry measurements were obtained using a conventional three-electrode cell with a Metrohm double junction Ag/AgCl reference electrode, glassy carbon working electrode (0.07 cm²) and Pt wire auxiliary electrode, under an argon atmosphere. [N(C₄H₉-*n*)₄]BF₄⁷ was used as the supporting electrolyte in acetonitrile that was freshly distilled (from CaH₂). Solutions containing ca.

10^{-3} M analyte (0.1 M electrolyte) were degassed by purging with nitrogen. All $E_{1/2}$ values were calculated from $(E_{pa} + E_{pc})/2$ at a scan rate of 100 mV s^{-1} and referenced to Fc/Fc⁺. Bulk electrolysis measurements were carried out using a similar cell adapted with a port to allow headspace sampling via a septum and a closable connection between working and reference compartments. This facilitates evacuation, backfilling and degassing of the cell while permitting separation of the compartments during electrolysis runs. The working electrode was a glassy carbon block suspended from a clip using copper tape (wrapped with PFTE kept above the level of the electrolyte), the total working area exposed to the electrolyte was *ca.* 3 cm^2 . Catalyst and acetic acid were added to achieve concentrations in the 5 mL working electrode solution of 0.2 mM and 40 mM respectively. Electrolysis was performed with stirring at the potential corresponding to half of the maximum current of the electrocatalytic wave, as determined by CV. This corresponded to -1.5 V for **1** and -1.68 V for **2** (*vs* Ag/AgCl reference, this is -1.87 and -2.05 V *vs* the Fc/Fc⁺ used to reference the cyclic voltammograms). The working compartment headspace was sampled for H₂ by gas chromatography every 350 s until completion of the run at 2100 seconds (35 minutes), the quantity of H₂ present was calculated using a direct calibration of the cell obtained by injecting known quantities of H₂ into the headspace of the same cell with the same quantity of electrolyte present. A leak test showed only a small decline (5%) in a gas chromatograph reading of 500 mVs for the cell left over a 30 minute period, indicating that loss of H₂ is only a small error in these measurements.

Isolation of Ethylamine (and trace amines) as 2,4-dinitrophenyl derivatives

Concentrated (37%) HCl (0.1 mL) was added to the working (cathode) compartment while still sealed, and the solution rapidly stirred for several minutes at the end of the bulk electrolysis to prevent escape of volatile amine products upon opening. The catholyte solution was transferred to a round-bottomed flask, water (2.5 mL), 2,4-dinitrofluorobenzene (0.037 g) and NaHCO₃ (0.3031 g) were added, and the resulting mixture stirred at 60 °C for one hour, then overnight at room temperature. 5 M aqueous NaOH (1 mL) was added to the resulting yellow solution, which became orange upon stirring at 60 °C for a further hour. Upon cooling, two phases formed. The lower aqueous phase was separated and extracted with diethyl ether (2 × 15 mL). The diethyl ether layers were recombined with the first organic fraction and these combined orange organic layers were washed with one portion of water (20 mL), and then repeatedly with 0.36 M aqueous NaHCO₃ until colour stopped moving from the organic to the aqueous layer. The resulting yellow organic layer was dried over MgSO₄, filtered and evaporated to dryness. Quantities of ethylamine were determined in CD₃CN by comparison of ¹H-NMR integrals to known quantities of added trimethoxybenzene (1 to 3 mg), and the spectra of authentic samples. Testing this method on a known quantity (4 mg) of ethylamine hydrochloride indicated that 87% of the ethylamine was isolated in the ¹H-NMR sample as its 2,4-dinitrophenyl derivative. This factor of 0.87 was used to adjust the reported Faradaic yields of ethylamine.

X-ray Crystallographic Details

Sample Growth, Data Collection and Refinement. Crystals of **1** and **2** were grown by vapour diffusion of diethyl ether into methanol. For **1** data were collected on a Rigaku AFC 12 goniometer equipped with an enhanced sensitivity (HG) Saturn724+ detector and FR-E+ SuperBright molybdenum rotating anode generator with HF Varimax optics (100 μm focus), and for **2** an Oxford Diffraction XCalibur 3 diffractometer. Data reduction, cell refinement and absorption correction was carried out using Agilent Technologies⁸ or Rigaku⁹ CrysAlisPro software. The structures were solved using SHELXT-2015¹⁰ via Olex2¹¹ (**1**) and SHELXS-2014¹² via WinGX (**2**).¹³ Refinement was achieved by full-matrix least-squares on all F_0^2 data using SHELXL-2014¹⁴ and molecular graphics were prepared using ORTEP-3¹⁵ or Mercury 3.8.¹⁶ In **1** disorder of the ligand over a two-fold rotation axis required

the use of restraints on the overlapping pyridine rings. Full crystallographic data and refinement details are presented in Table S1 and ORTEP representations of the two structures in Figures S1 and S2.

Table S1. Crystallographic Data and Refinement Details for **1** and **2**

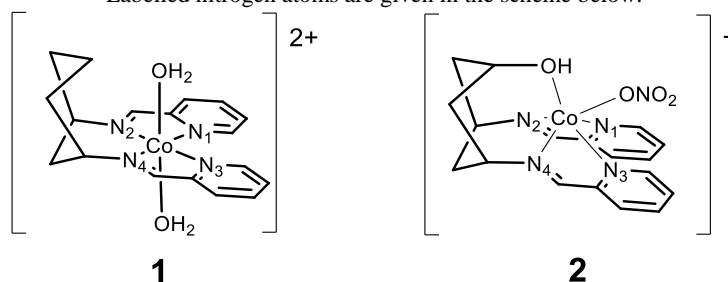
	1	2
Formula	C ₁₈ H ₂₄ CoN ₆ O ₈	C ₁₈ H ₂₀ CoN ₆ O ₇
<i>M</i>	511.36	491.33
cryst syst	monoclinic	monoclinic
space group	C2/c	P21/n
<i>a</i> /Å	14.6698(4)	8.774(1)
<i>b</i> /Å	10.0506(2)	18.751(2)
<i>c</i> /Å	16.0714(4)	12.185(1)
<i>α</i> /deg	90	90
<i>β</i> /deg	116.734(3)	101.49(1)
<i>γ</i> /deg	90	90
<i>U</i> /Å ³	2116.3(1)	1964.6(4)
<i>Z</i>	4	4
<i>T</i> /K	100(2)	140(2)
<i>μ</i> /mm ⁻¹	0.871	0.931
Cryst. size/mm	0.24 × 0.18 × 0.03	0.27 × 0.16 × 0.08
Cryst. description	Orange plate	Brown block
<i>λ</i> /Å	0.71073	0.71073
No. reflns collected	13100	30991
No. of indep. reflns (<i>R</i> _{int})	2431 [R(int) = 0.0172]	4507 [R(int) = 0.0307]
<i>θ</i> _{max} /deg (completeness)	27.481 (99.8%)	25.24 (99.8%)
Reflections with <i>I</i> > 2σ(<i>I</i>)	2336	3962
Goodness-of-fit on <i>F</i> ²	1.083	1.080
final <i>R</i> ₁ , <i>wR</i> ₂ [<i>I</i> > 2σ(<i>I</i>)] ^a	<i>R</i> ₁ = 0.0224, <i>wR</i> ₂ = 0.0587	<i>R</i> ₁ = 0.0300, <i>wR</i> ₂ = 0.0743
(all data)	<i>R</i> ₁ = 0.0224, <i>wR</i> ₂ = 0.0235	<i>R</i> ₁ = 0.0370, <i>wR</i> ₂ = 0.0770
Peak and hole/e Å ⁻³	0.282 and -0.237	0.411 and -0.301

Table S2. Coordinate bond lengths of **1** and **2**

Compound	Iminopyridine arm (1)		Iminopyridine arm (2)		<i>R</i> _{M-O} /Å		
	Length/Å		Length/Å		Water	Nitrate	Hydroxyl
	M - N(1) Py	M - N(2) Im	M - N(3) Py	M - N(4) Im			
1	2.118(1)	2.123(3)	2.194(1)	2.103(3)	2.085(1) ¹	-	-
2	2.176(4)	2.142(14)	2.205(4)	2.116(5)	-	2.117(3)	2.075(2)

¹1-X,+Y,1/2-Z (symmetry generated)

Labelled nitrogen atoms are given in the scheme below.



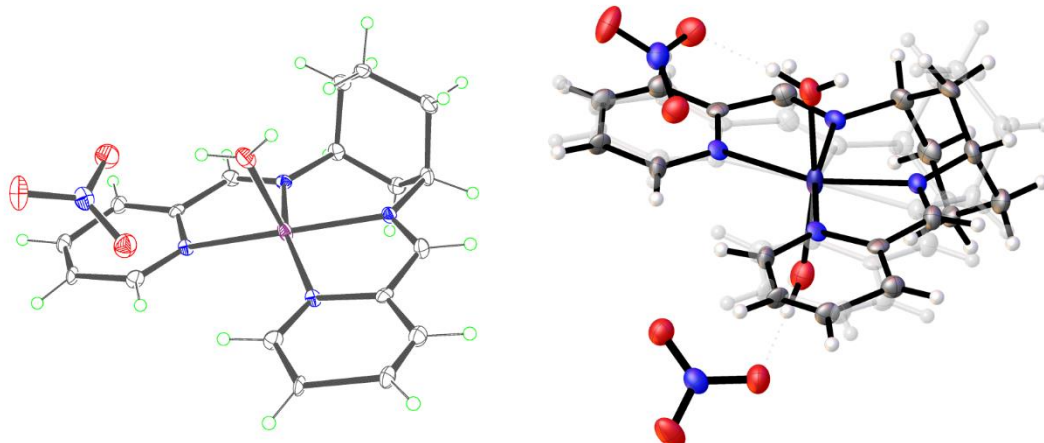


Figure S1. **Left** – ORTEP representation of the asymmetric unit of **1**. Thermal ellipsoids are at the 30% probability level: C is grey; O, red; N, blue; Co, purple; H atoms are green circles of arbitrary radii. **Right** – disorder of the entire structure of **1** across a two-fold rotation axis. Thermal ellipsoids are at the 50% probability level.

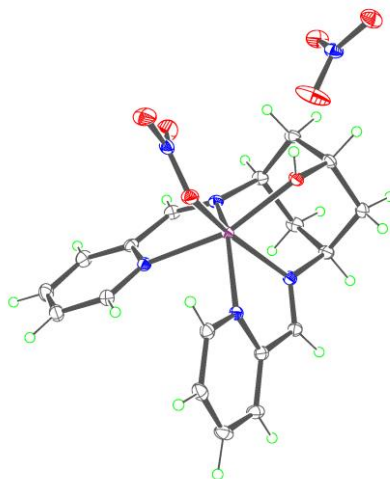


Figure S2. ORTEP representation of the asymmetric unit of **2**. Thermal ellipsoids are at the 30% probability level: C is grey; O, red; N, blue; Co, purple; H atoms are green circles of arbitrary radii.

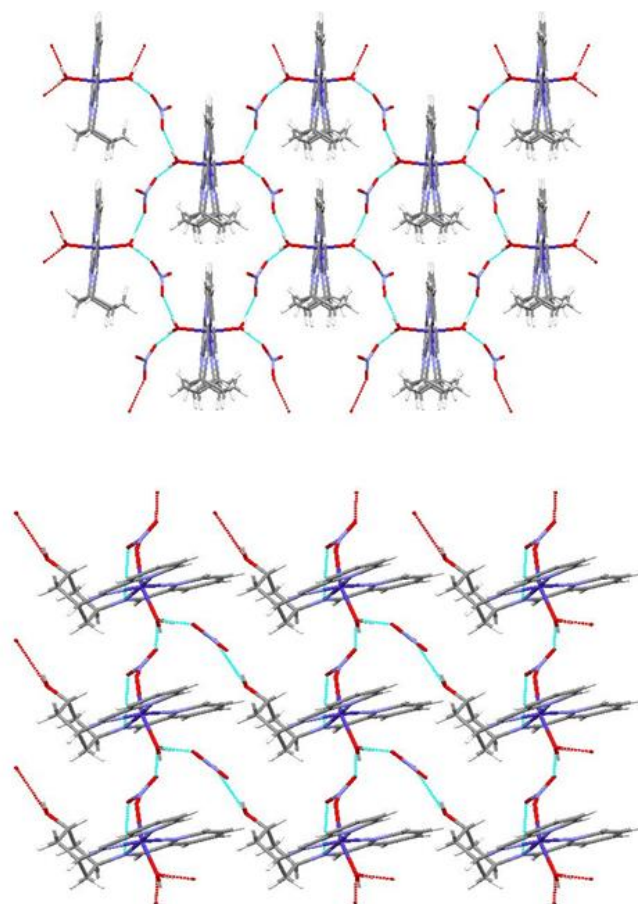


Figure S3. Top: 2-dimensional hydrogen bonded network of **1** viewed in the crystallographic *ac* plane. Hydrogen bonds are shown as bright blue lines. **Bottom:** 2-dimensional hydrogen bonded network of the previously published *trans*-hydroxy derivative,¹⁷ also viewed in the *ac* plane. Formation of these networks is the likely driving force for coordination of two aqua ligands in **1**, as opposed to one nitrate- and one aqua-ligand in the *trans*-hydroxy compound.

Paramagnetic ¹H-NMR

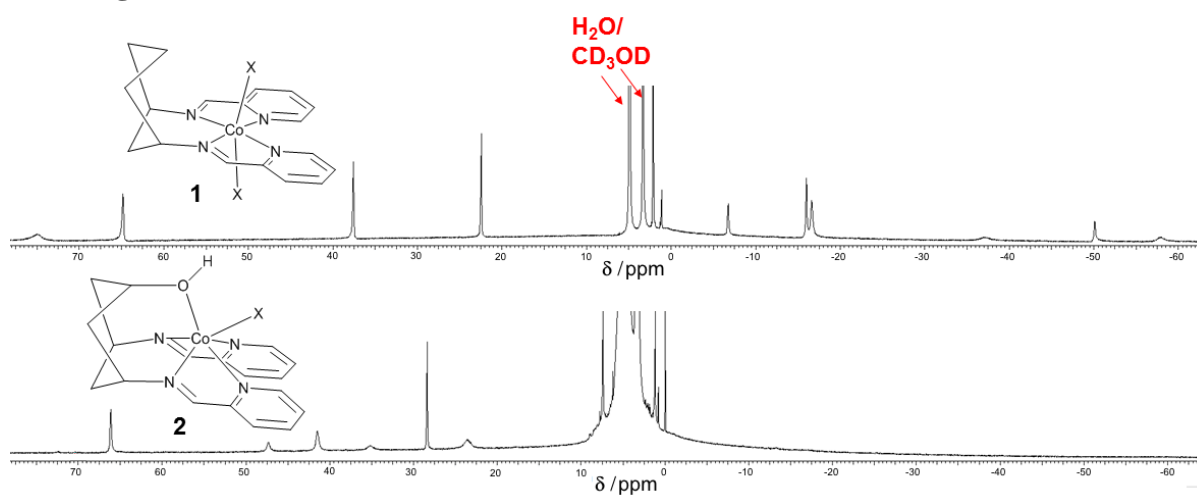


Figure S4. Paramagnetic ¹H-NMR spectra of **1** and **2**. Environments with negative chemical shifts in **1** shift and appear to cluster close to the solvent / water peaks, indicating the structural difference between the two complexes is retained in solution, even in a coordinating solvent (CD₃OD).

Computational Details

DFT calculations were performed using the Gaussian 09 suite of programs.¹⁸ Structures were optimized in the gas phase using the PBE¹⁹ functional from crystal structures obtained in the Co^{2+} oxidation state (referred to as the 0 state in the main paper, Fig. 2). These structures were then used as a starting point for calculation of optimized acetonitrile solution structures of the 0, -1, -2 and -3 states, with the solvent introduced using the SMD solvent scheme.²⁰ In each case, carbon nitrogen and hydrogen were treated with the 6-311g(d,p) basis set with metal centres described with the lanl2dz²¹ basis set with effective core potential. All structures were confirmed as minima by frequency analysis. Diagrams showing the complexes and HOMO and LUMO molecular orbitals were then generated using Gaussview (Figure S5, below).

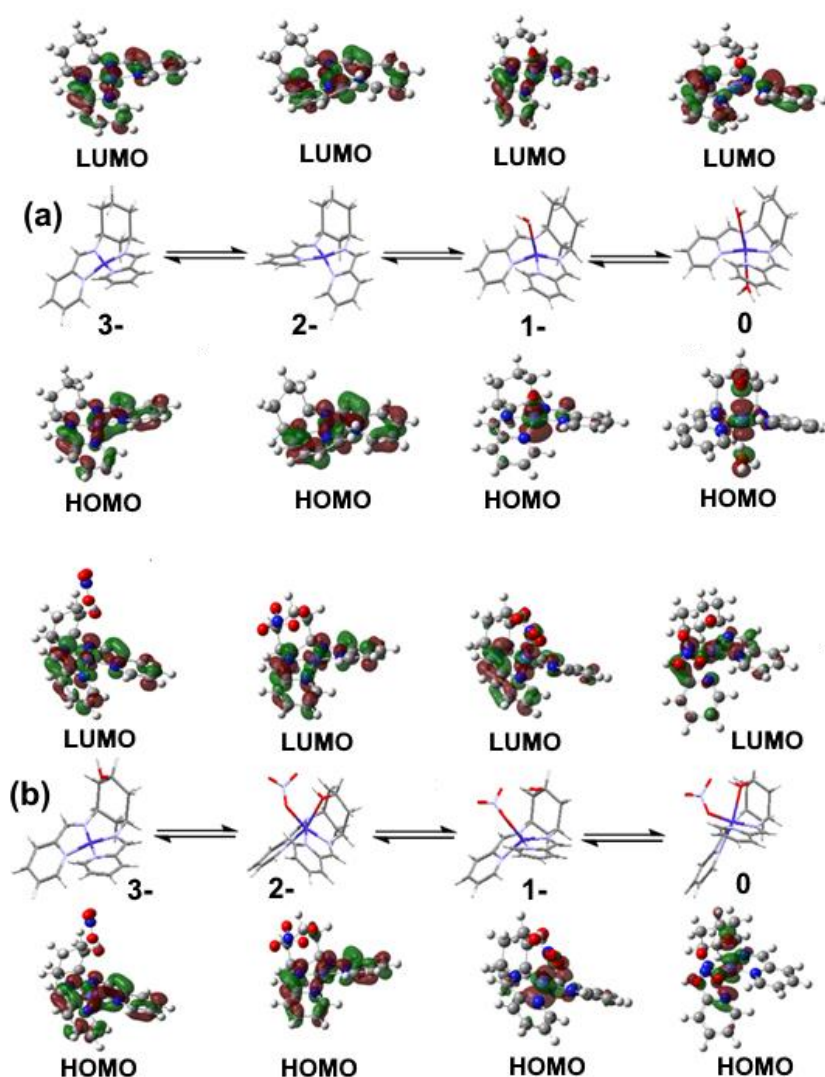


Figure S5. DFT calculated structures and frontier orbitals of **1** and **2** from starting Co^{2+} oxidation state (0), through the three quasi-reversible reductions.

Additional Cyclic Voltammograms

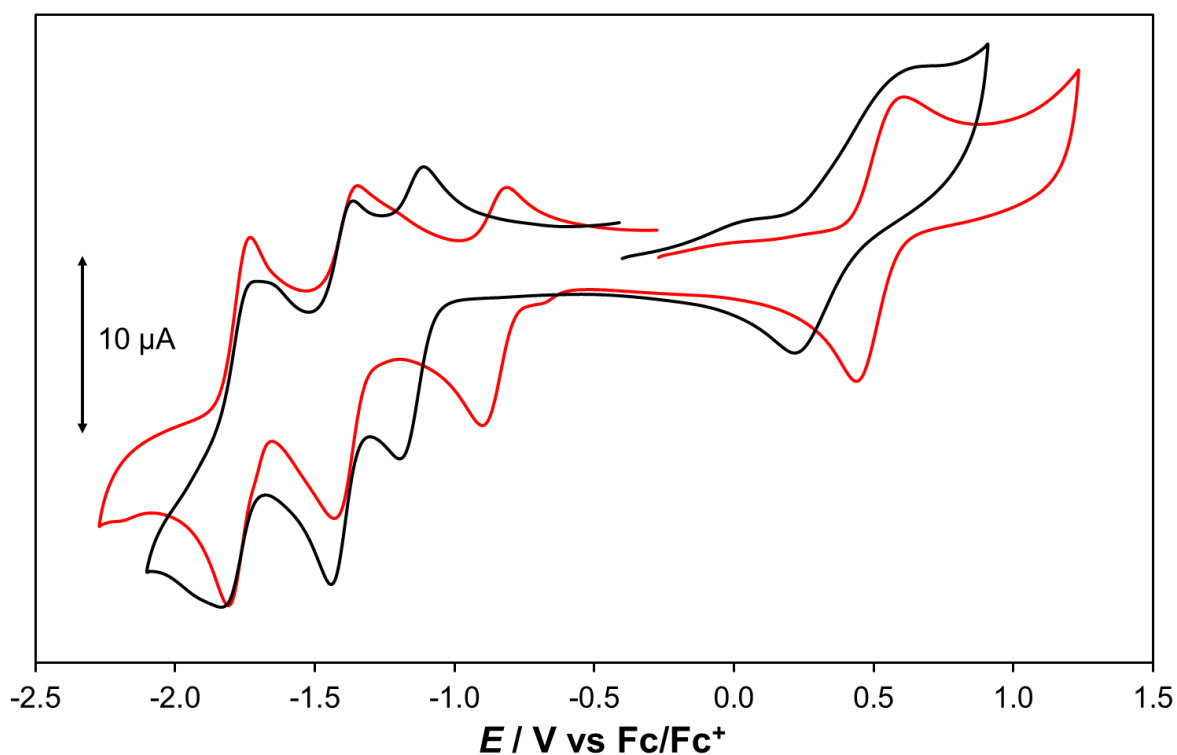


Figure S6. CV of 1 mM **1** (red) and **2** (black) at GCE in MeCN, at 100 mV s^{-1} . RE = $Ag/AgCl$ (internal Fc/Fc^+ reference), CE = Pt. 0.1 M TBABF_4 supporting electrolyte.

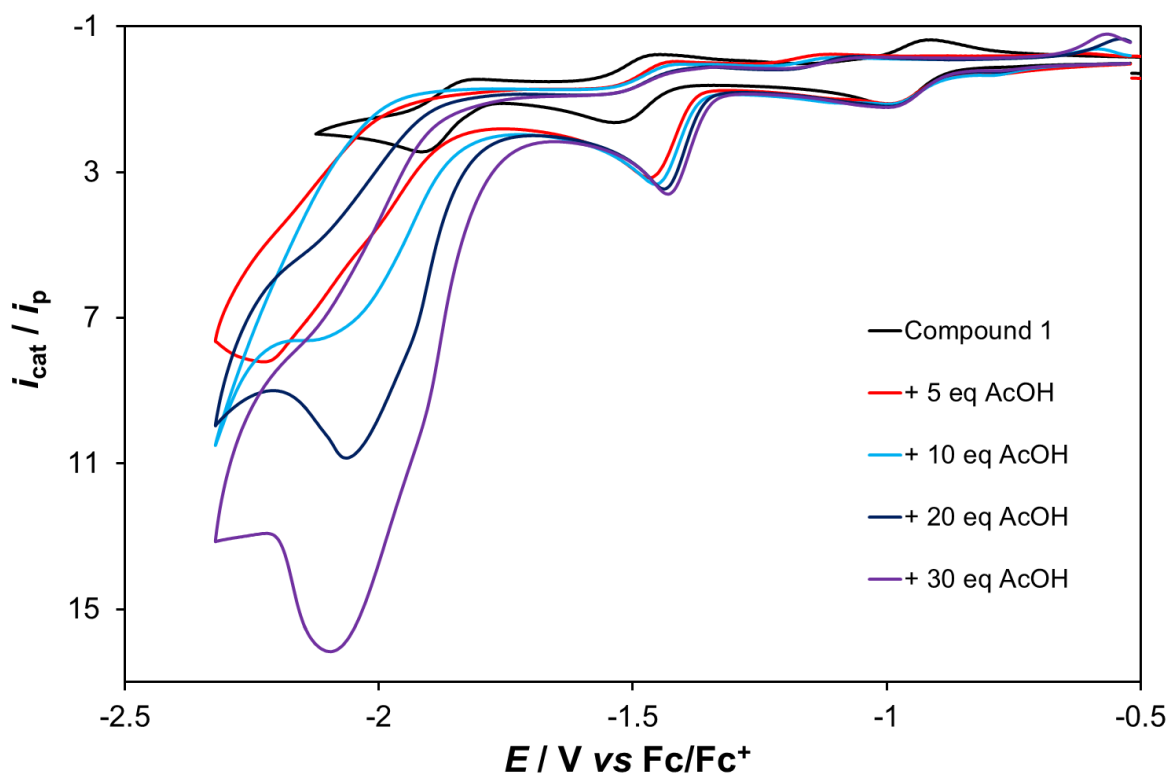


Figure S7. CV of 1 mM **1** with addition of 5 to 30 eq of AcOH at GCE in MeCN, at 100 mV s^{-1} . RE = $Ag/AgCl$ (internal Fc/Fc^+ reference), CE = Pt. 0.1 M TBABF_4 supporting electrolyte. Current has been normalised to the reductive current of the one electron waves observed in the complex with no acid added.

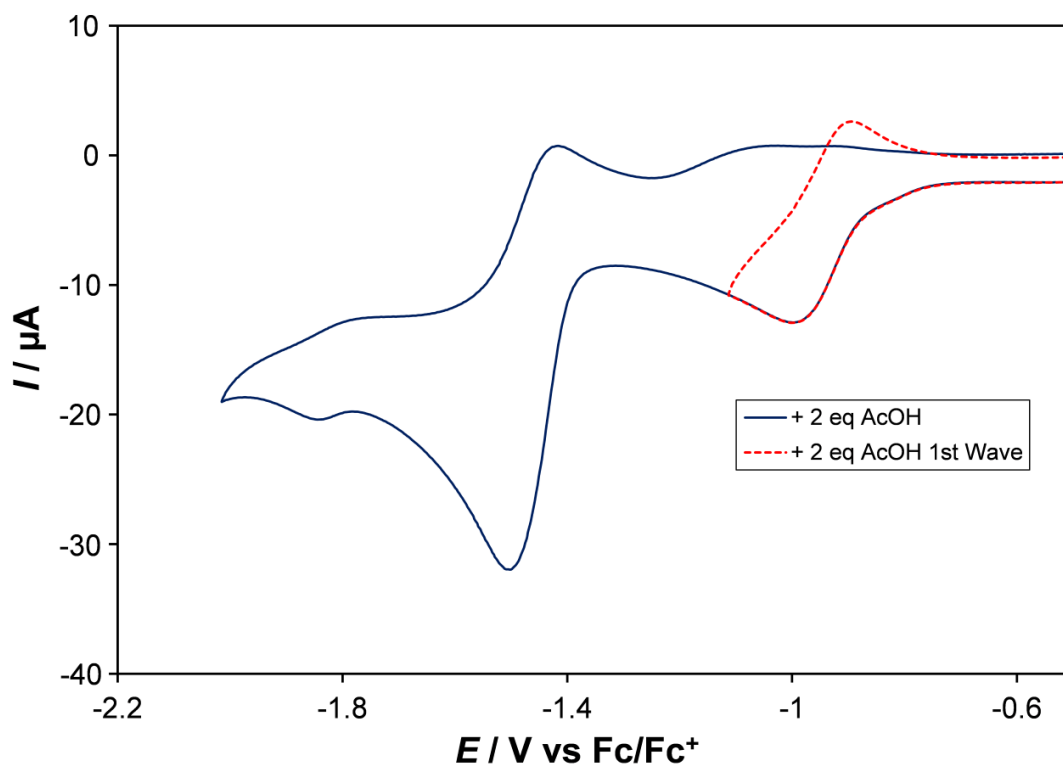


Figure S8. CV of 1 mM **1** with addition of 2 eq of AcOH at GCE in MeCN, at 100 mV s^{-1} . RE = Ag/AgCl (internal Fc/Fc⁺ reference), CE = Pt. 0.1 M TBABF₄ supporting electrolyte. Scanning only the first reduction wave results avoids the changes to the potential of the return wave, indicating that chemical changes to **1** must occur on the second and third waves.

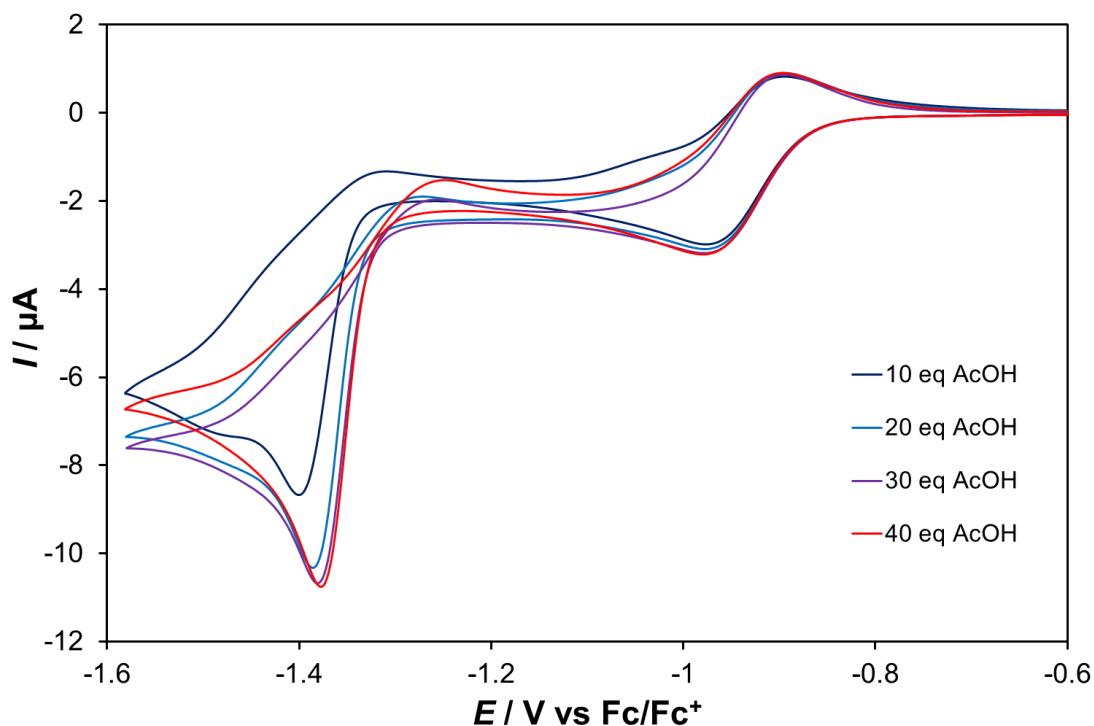


Figure S9. CV of 0.6 mM **1** with addition of 10 to 40 eq of AcOH at GCE in MeCN, at 10 mV s^{-1} . RE = Ag/AgCl (internal Fc/Fc⁺ reference), CE = Pt. 0.1 M TBABF₄ supporting electrolyte. The persistent reversibility of the first wave at low scan rate, coupled with the growth of the second wave with addition of more AcOH, indicate that the second wave involves a slow catalytic process in the presence of acid.

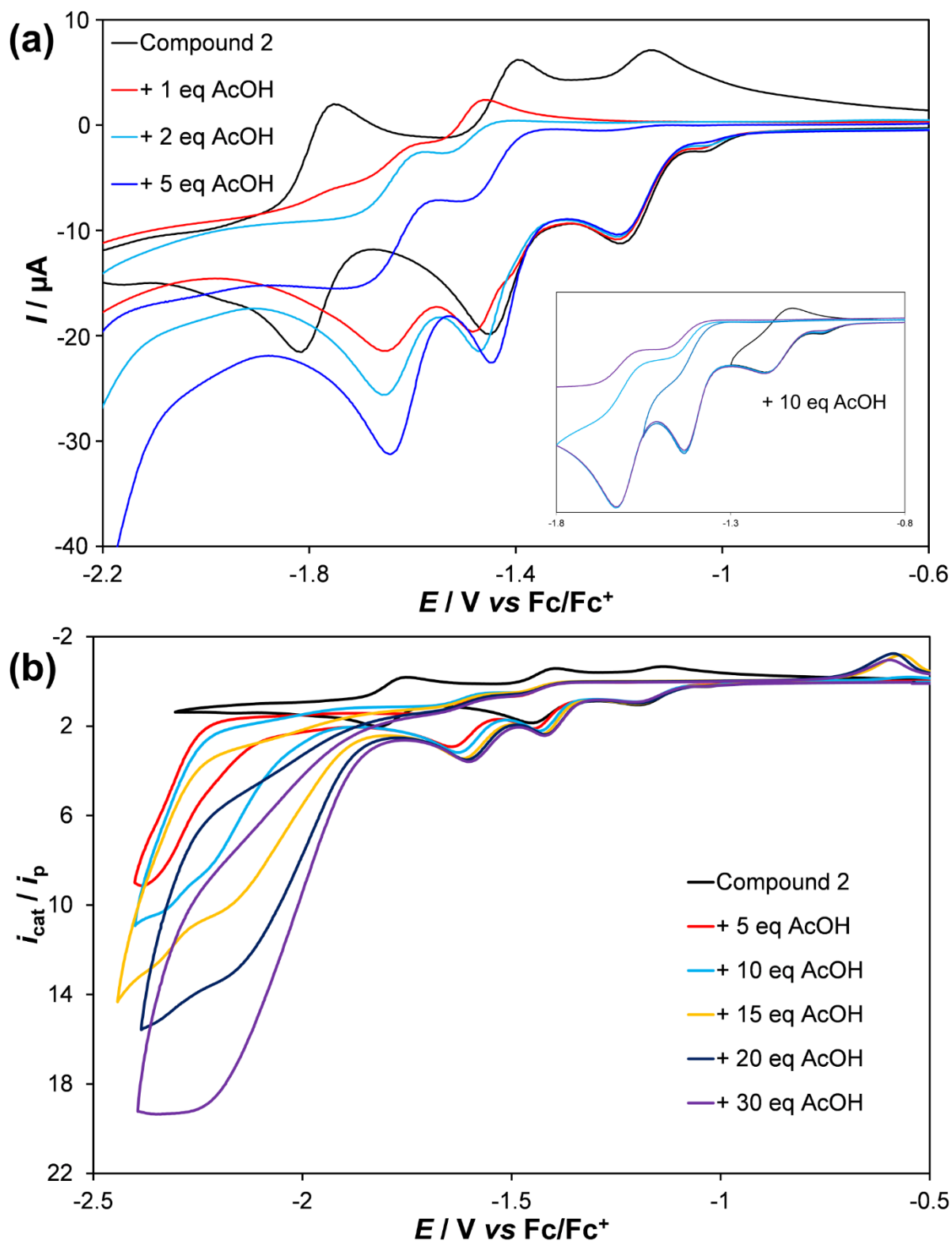


Figure S10. CV of 1 mM **2** with addition of AcOH at GCE in MeCN, at 100 mV s⁻¹. **(a)** Expansion of the first three reduction waves showing response to addition of acid. Inset shows that first wave remains quasi-reversible if scanned in isolation, irreversible chemical change happens on the second wave. **(b)** Full range showing development of the catalytic wave. RE = Ag/AgCl (internal Fc/Fc⁺ reference), CE = Pt. 0.1 M TBABF₄ supporting electrolyte. Current has been normalised to the current of the reductive one electron waves observed in the complex with no acid added.

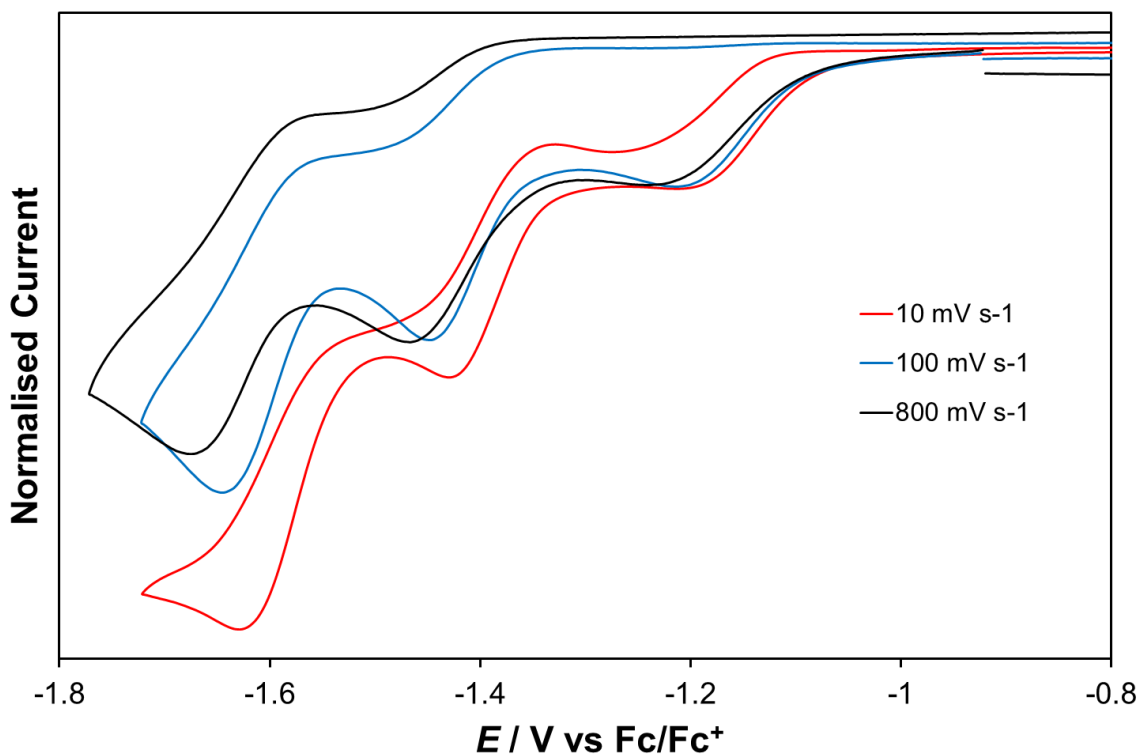


Figure S11. CV of 0.6 mM **2** with addition of 10 eq AcOH at GCE in MeCN, at 10, 100 and 800 mV s^{-1} . RE = Ag/Ag^+ (internal Fc/Fc^+ reference), CE = Pt. 0.1 M TBABF₄ supporting electrolyte. Current has been normalised for scan rate so that the first wave has the same reduction peak current at all scan rates. As for **1**, increased current enhancement of the PCET waves at *ca.* -1.4 and -1.6 V and increased reversibility of acid independent Co^{III} couple is evident at low scan rates, implying the PCET waves involve slow catalysis.

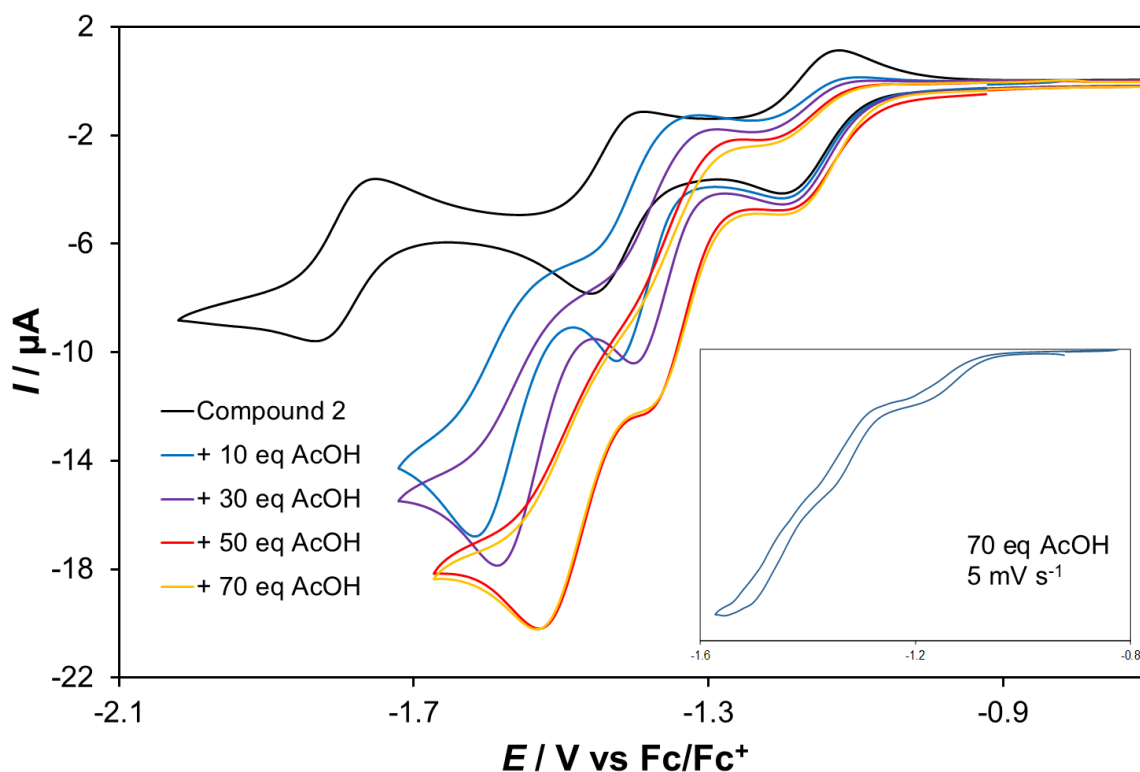


Figure S12. CV of 0.6 mM **2** with addition of 0 to 70 eq AcOH at GCE in MeCN, at 25 mV s^{-1} . Inset – with 70 eq AcOH at 5 mV s^{-1} . RE = Ag/Ag^+ (internal Fc/Fc^+ reference), CE = Pt. 0.1 M TBABF₄ supporting electrolyte.

Post-Reaction Cyclic Voltammograms

The three cycle CVs below show that after a single scan of the catalytic wave, the $\text{Co}^{\text{I}}/\text{Co}^{\text{II}}$ process shifts (**1**, Fig. S13) or disappears under the subsequent (more negative) reduction process (**2**, Fig. S14). Retention of the imine reduction process is consistent with the slow H_2 evolution – e.g. trapping of the reduced ligand species in the Co^{II} oxidation state in the reoxidation cycle, and then liberation of H_2 upon reduction back to Co^{I} . There is then little change between the second and third scans. However, after bulk electrolysis (Fig. S15) the similarity to the CV of a bulk electrolysed blank system means that there is little evidence of these (or other) electroactive molecular species in the catholyte at the end of reaction. This implies irreversible degradation of **1** and **2**, apparently to inactive materials. Moreover, bulk electrolyses conducted with the resulting fouled electrodes (Table S3) do not produce ethylamine.

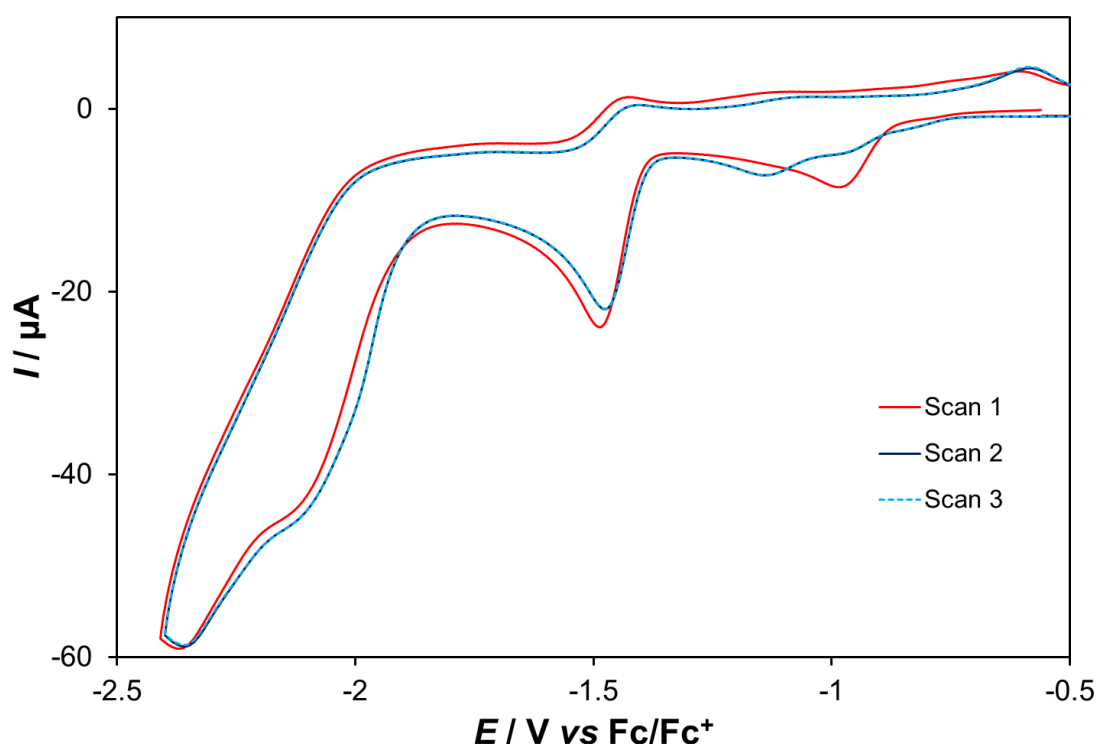


Figure S13. Consecutive cyclic voltammograms of 0.6 mM **1** in the presence of 10 eq AcOH. GC working electrode, RE = Ag/AgCl, CE = Pt. 0.1 M TBABF₄ supporting electrolyte in MeCN, scan rate 100 mV s⁻¹.

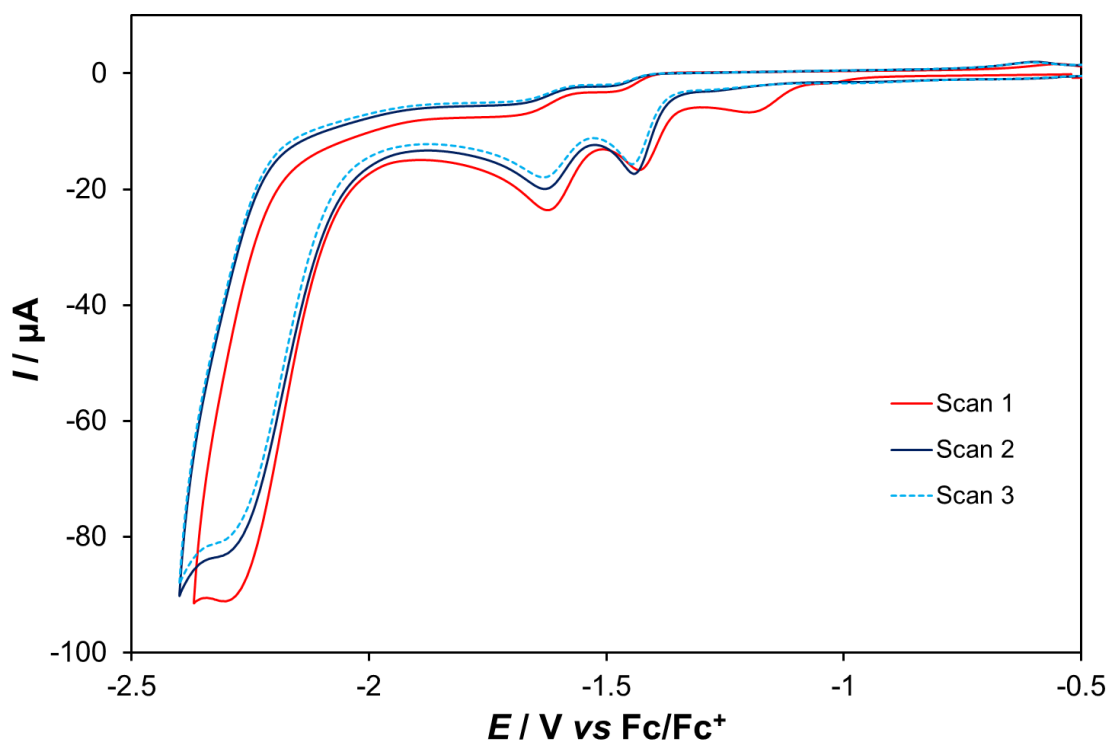


Figure S14. Consecutive cyclic voltammograms of 0.6 mM **2** in the presence of 10 eq AcOH. GC working electrode, RE = Ag/AgCl, CE = Pt. 0.1 M TBABF₄ supporting electrolyte in MeCN, scan rate 100 mV s⁻¹.

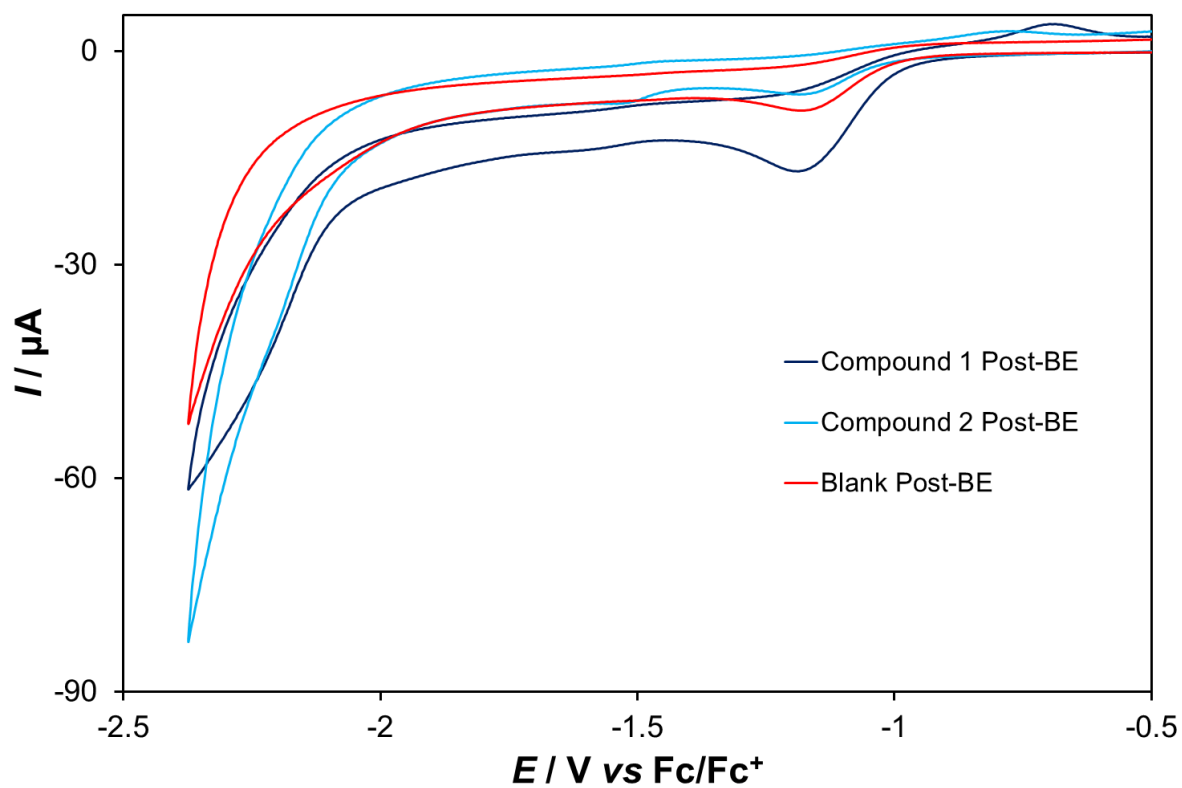


Figure S15. Post-bulk electrolysis cyclic voltammograms of **1**, **2** and a blank, with a clean GC voltammetry electrode. RE = Ag/AgCl, CE = Pt. 0.1 M TBABF₄ supporting electrolyte in MeCN, scan rate 100 mV s⁻¹.

Calculation of Turnover Frequency, TOF

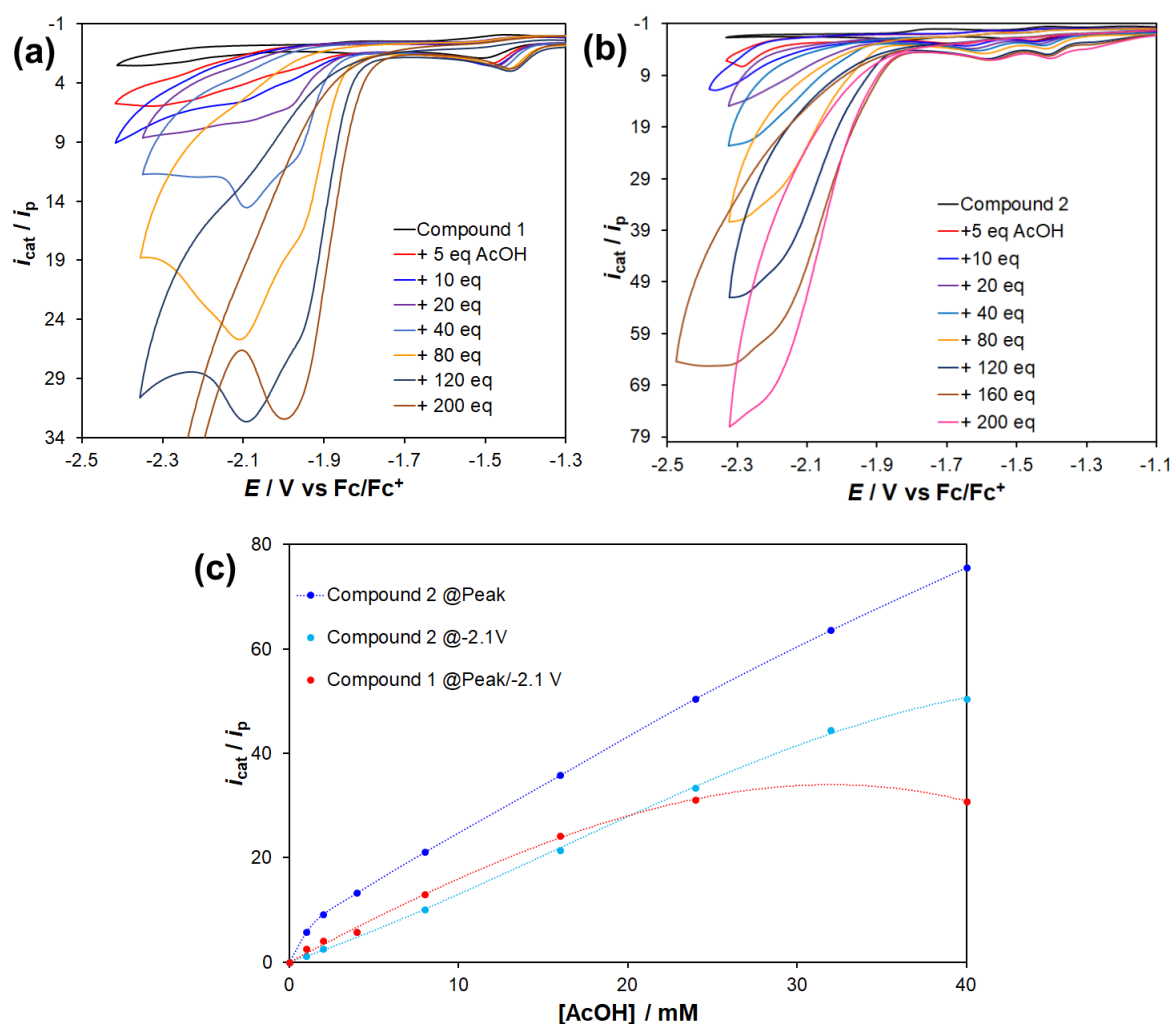


Figure S16. (a and b) Response of **1** and **2** (0.2 mM) to acetic acid in acetonitrile at a GC electrode, scan rate 100 mV s^{-1} , area 0.07 cm^2 (b) Plot of normalised catalytic current (i_{cat}/i_p) vs concentration of acid. Data for **1** is taken at -2.1 V up until 20 eq AcOH), and thereafter at the peak. Data taken at the peak of **2** is likely to be quite strongly affected by direct reduction of AcOH, and EtNH_2 has not been quantified at higher voltages. Thus, data at -2.1 V is also plotted to provide a fairer comparison with **1**.

Calculation of the ethyl amine turnover frequency (TOF) for **1** and **2** was performed by first multiplying the peak i_{cat}/i_p by the faradaic efficiency calculated in bulk electrolyses, to estimate the current resulting from ethyl amine production. Because of possible contributions from AcOH reduction by the electrode, data was taken at -2.1 V if the peak occurred above -2.1 V . However, as shown in Table S2 below, even at high potentials (up to -2.3 V), low faradaic efficiencies for H_2 indicate that most of the current is from molecular catalyst-based processes.

The faradaic efficiency adjusted i_{cat}/i_p was then used to calculate the TOF using the formula below:

$$\frac{i_{cat}}{i_p} = \frac{n}{0.4463} \sqrt{\frac{RT(TOF)}{Fv}}$$

Where n is the number of electrons in the process, R is the ideal gas constant, T is temperature, F is the Faraday constant and v is the scan rate in V s^{-1} .

For a four-electron process, such as reduction of ethyl amine, this simplifies to:

$$TOF = k_{obs} = v \left(\frac{i_{cat}}{i_p} \right)^2$$

Strictly, as **2** has not reached a plateau a first order rate constant should be reported, rather than a zero-order turnover frequency. However, in the manuscript we report a TOF for **2** under the specific bulk electrolysis conditions (40 mM AcOH) to facilitate comparison with **1**. Both estimates are likely conservative as we expect that the faradaic efficiency of EtNH₂ production is higher earlier in the BE run, and declines as **1** and **2** degrade.

Below, results are shown on H-terminated boron doped diamond (BDD), which has a lower activity for reduction of AcOH than glassy carbon (Fig S10d). These indicate that **2** can ultimately access much higher current densities than **1** and is a more active catalyst. Attempts to quantify ethylamine and H₂ production on BDD have however been prevented by degradation of the BDD wafer when biased to highly negative potentials over the long periods of time used in bulk electrolyses.²² This causes the electrode to become increasingly active for direct reduction of the acid.

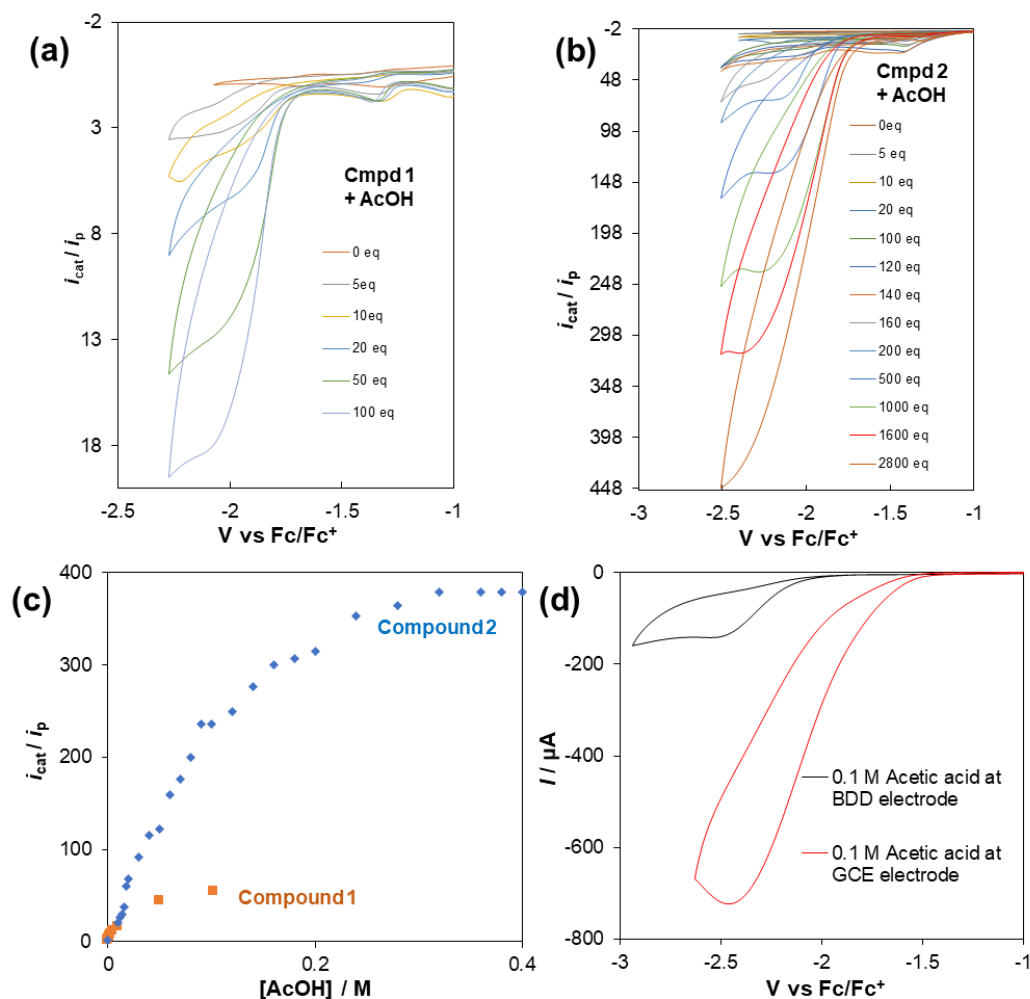


Figure S17. (a and b) Responses of **1** and **2** to higher concentrations of AcOH on 0.07 cm² BDD electrodes, concentration of catalyst 0.1 mM, scan rate 100 mV s⁻¹. (c) Plot of i_{cat}/i_p for **1** and **2** showing the plateau in activity for **2** occurs at much (7.6 ×) higher value of i_{cat}/i_p than for **1**. (d) Scan of AcOH (0.1 M) at both BDD and GC electrodes of equal area (0.07 cm²), showing weaker activity of BDD for direct acid reduction.

Additional Bulk Electrolysis Data

Table S2. Bulk electrolysis using electrodes fouled by **1** and **2** in the previous bulk electrolysis run.

	Yields of H ₂		EtNH ₂	3-aminocrotonitrile
	Faradaic	Chemical		
1 -fouled GC ^a	50%	21%	0	Trace
2 -fouled GC ^b	51%	23%	No data	No data

^aRun at potential used for bulk electrolysis with **1**, -1.5 V vs Ag/AgCl. ^bRun at potential used for bulk electrolysis with **2**, -1.68 V vs Ag/AgCl, amine isolation not attempted due to negative result with **1**.

Table S3. Bulk electrolysis conducted at higher potential – the peak of the catalytic wave for each catalyst as measured on the GC block electrode before the run.

Catalyst	E / V	Q / C	Yields of H ₂	
			Faradaic	Chemical
Blank ^a	-2.3	14.47	91%	69%
1	-2.1	18.68	28%	36%
2	-2.3	21.90	46%	53%

All systems 40 mM in AcOH, 0.2 mM in molecular catalyst in MeCN, 0.1 M NBu₄BF₄ supporting electrolyte

These data show the same basic trend in the behaviour of **1** and **2** with regard to hydrogen evolution is retained at more negative potential – **2** produces more hydrogen, but both produce much less H₂ than a GC electrode with no catalyst (blank) despite higher amounts of charge passed. This indicates that even at these high potentials, most of the current results from catalyst-based processes rather than reduction of AcOH by the electrode. The H₂ Faradaic yield for **1** doubles at the more negative potential, but the increase for **2** is smaller. This suggests that the source of the H₂ for **1** may only be direct reduction at the electrode, which increases sharply as potential becomes more negative, while for **2** participation of the catalyst seems likely. It is noteworthy that at the more negative potential, the Faradaic efficiency of direct H₂ production by the GC electrode approaches 100%. This may be because any current involved in reducing GC surface functionalities becomes proportionately smaller as the overall current increases.

Example $^1\text{H-NMR}$ Spectra

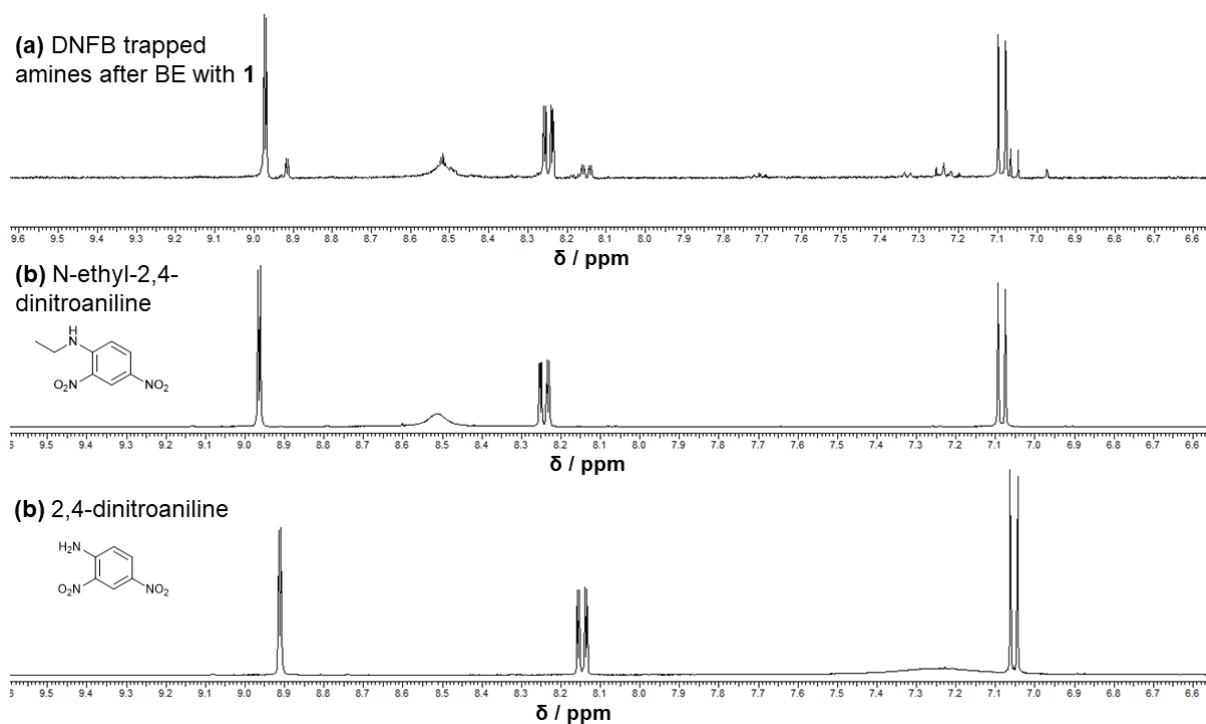


Figure S18. $^1\text{H-NMR}$ spectra in CD_3CN showing the aromatic region of a DNFB-treated bulk electrolysis run, vs products N-ethyl-2,4-dinitroaniline and 2,4-dinitroaniline.

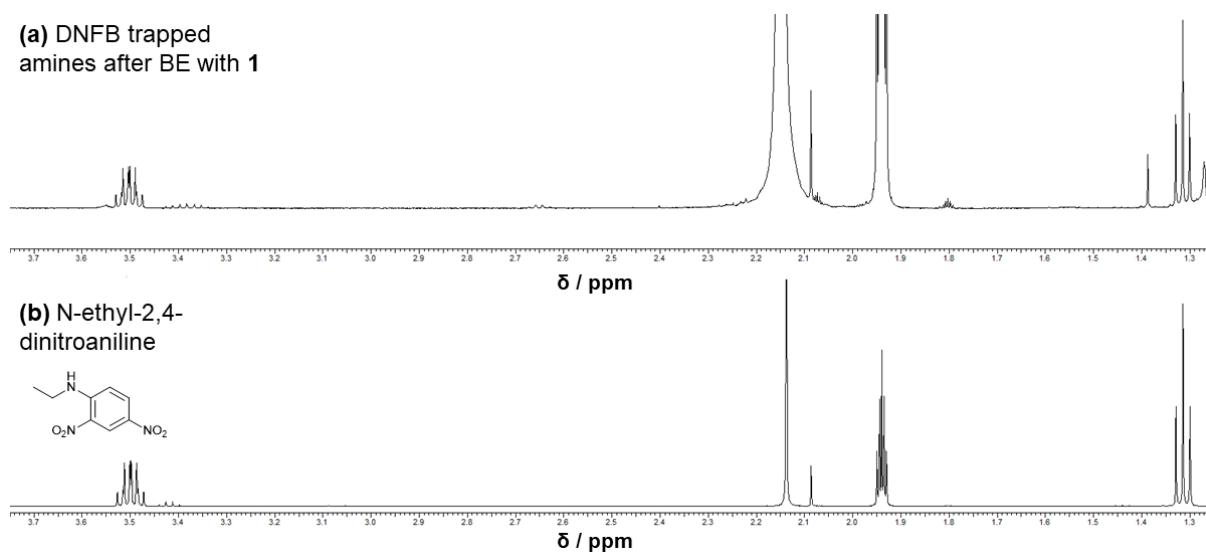
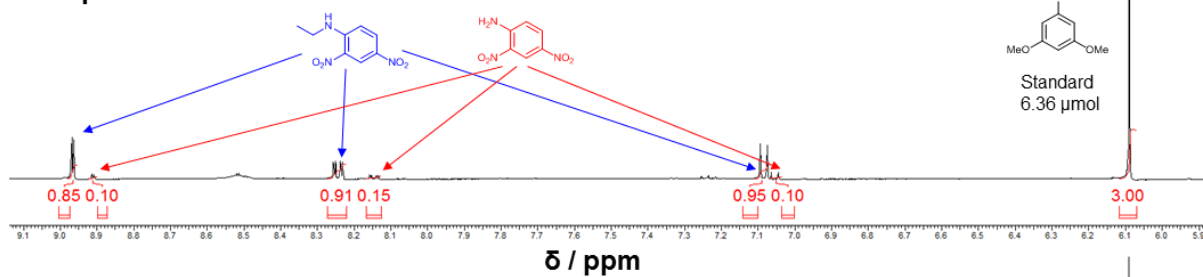


Figure S19. $^1\text{H-NMR}$ spectra in CD_3CN showing the aliphatic region of a DNFB-treated bulk electrolysis run, vs product N-ethyl-2,4-dinitroaniline.

NMR of DNFB trapped amines after BE
Compound 1



Compound 2

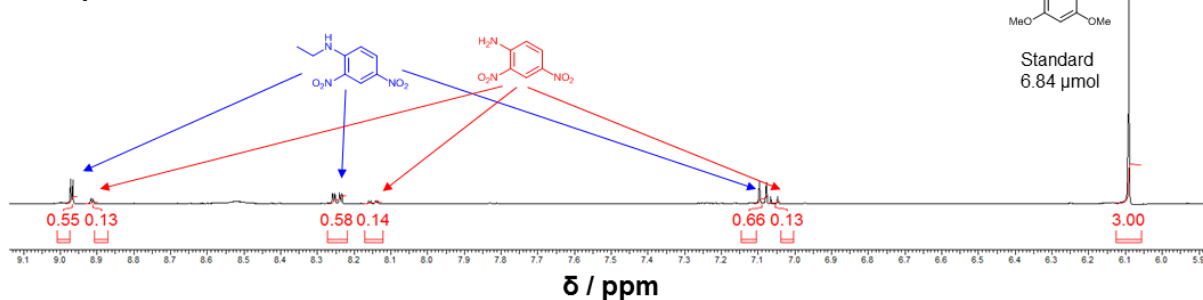


Figure S20. $^1\text{H-NMR}$ spectra in CD_3CN showing integration of the trapped amine products vs trimethoxybenzene standard, for bulk electrolyses performed with both **1** and **2**.

BE with 1 in CD_3CN , DCI added

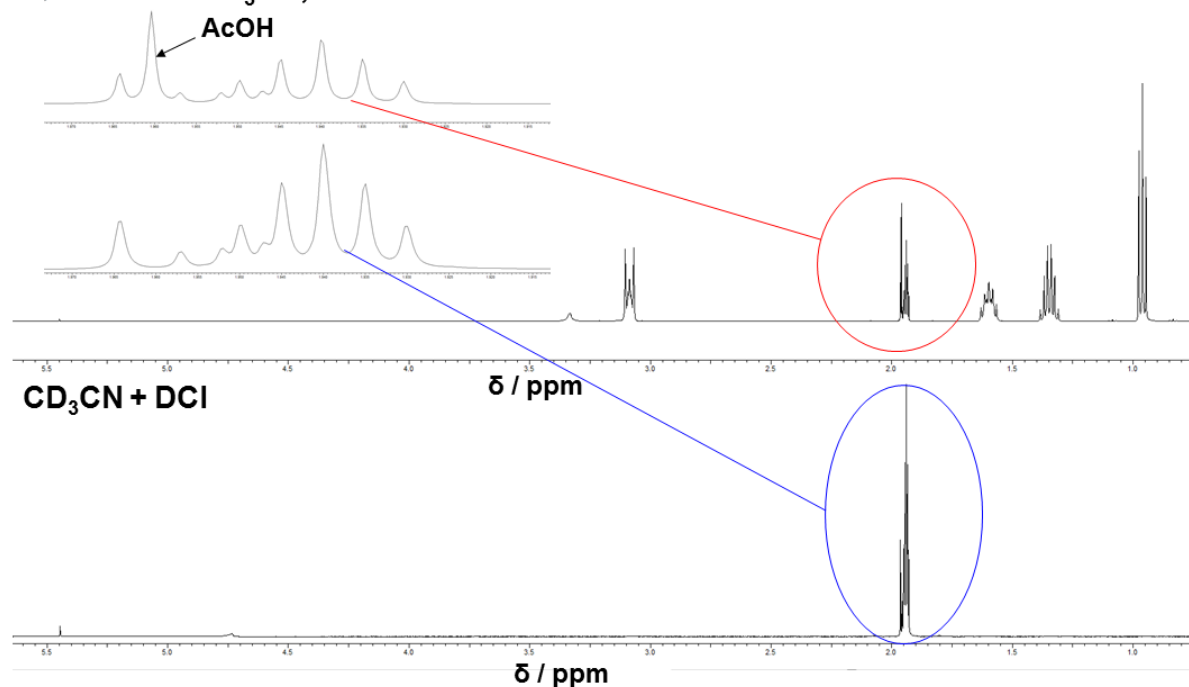


Figure S21. $^1\text{H-NMR}$ spectra of a bulk electrolysis performed in CD_3CN (**top**), run directly after addition of DCI to trap amines, compared with a blank of CD_3CN and DCI (**bottom**). The broad peaks at 3.35 and 4.5 ppm respectively result from residual H^+ whose chemical shift is highly dependent on the composition of the sample (presence of acetate and other anions).

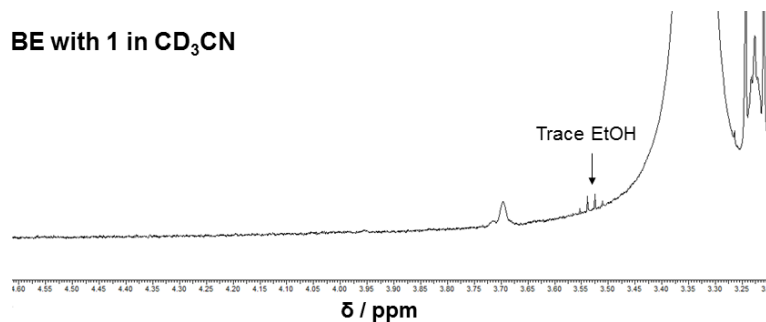


Figure S22. Trace ethanol signal observed in ¹H-NMR spectrum of a bulk electrolysis performed in CD₃CN. Integration and comparison to the residual acetic acid signal indicates that if a reaction product, it can account for no more than around 1% of the charge passed.

Mass Spectra

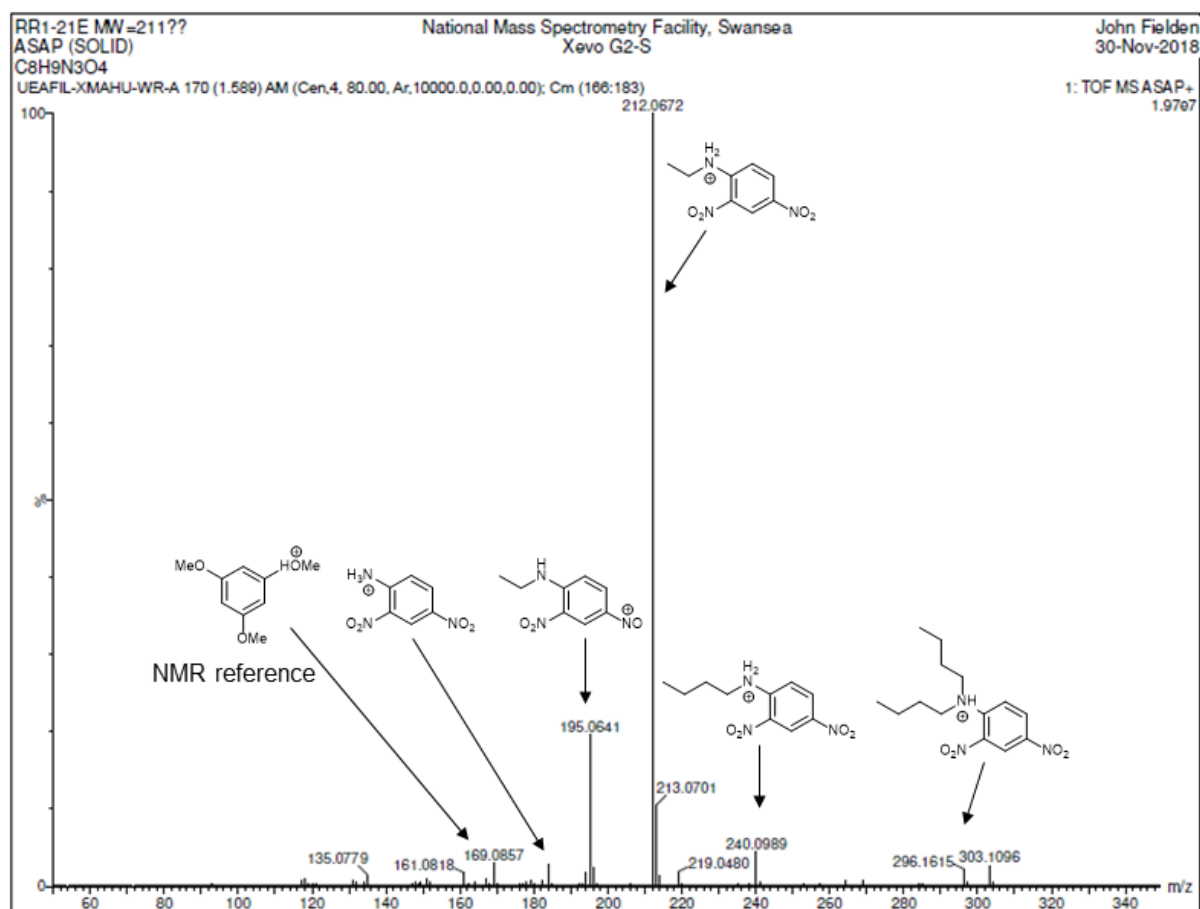


Figure S23. Assigned mass spectrum of the catholyte from bulk electrolysis with **1**, after treatment with DNFB.

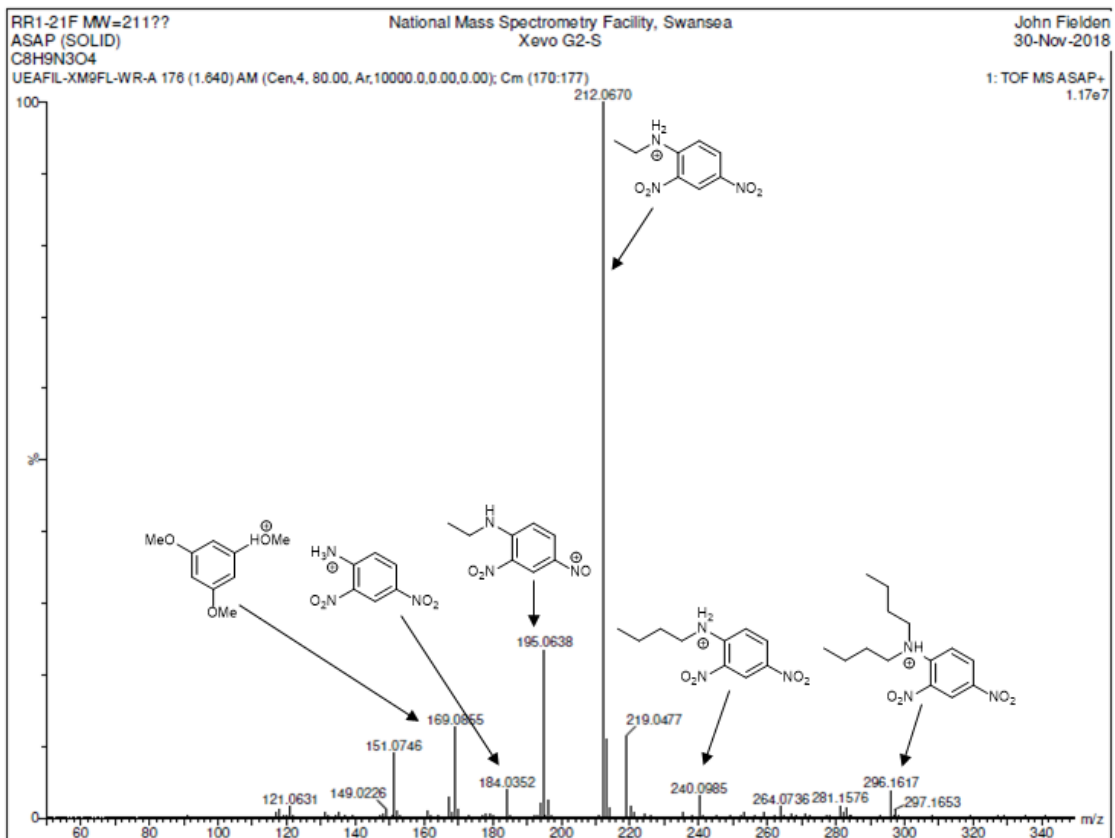


Figure S24. Assigned mass spectrum of the catholyte from bulk electrolysis with **2**, after treatment with DNFB.

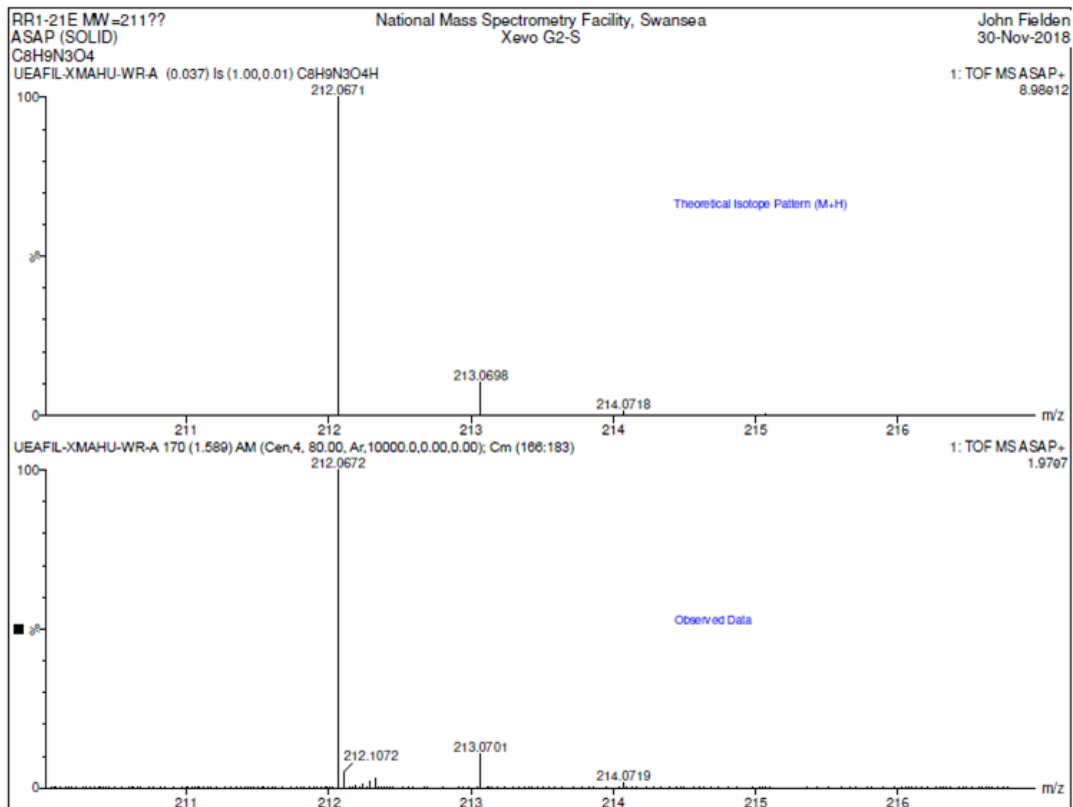


Figure S25. Theoretical vs observed isotope match for the peak at $m/z = 212.067$, confirming the ethylamine adduct.

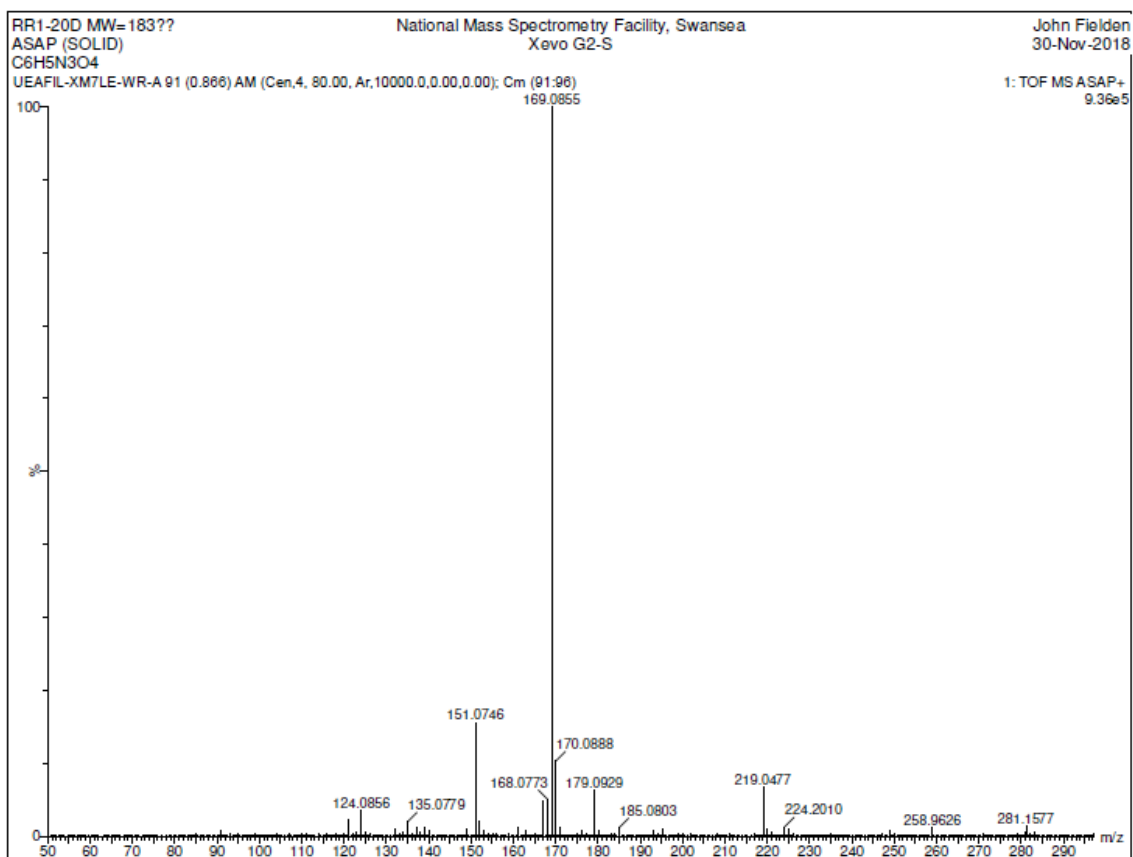
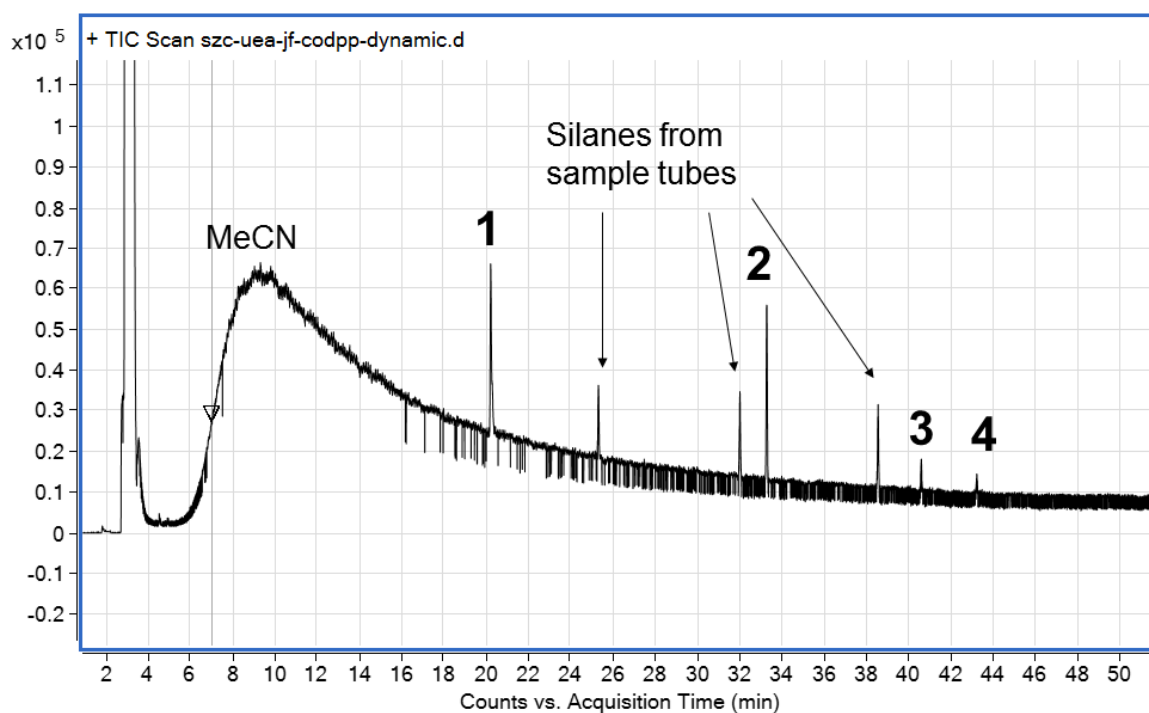


Figure S26. Mass spectrum of the catholyte from bulk electrolysis with no catalyst, after treatment with DNFB. None of the identified peaks from the bulk electrolyses with catalyst are present, apart from the $^1\text{H-NMR}$ reference, but several of the unidentified peaks in the spectra from the bulk electrolyses are also seen in this blank.

Gas Chromatography – Mass Spectrum



Peak	Best match	Match to retrn.	EI Mass spectrum	Likely Origin
1		97.9%		Reaction of MeCN
2		33.5% (also fits TBA salts)		Reaction of NBu ₄ ⁺
3		47.0%		Reduction of glassy carbon surface functionality
4		59.3%		Impurity in NBu ₄ BF ₄

Figure S27. GC-MS of untreated (no DNFB) catholyte from bulk electrolysis with **1**. Conditions are optimised for higher molecular weight products – ethylamine is not observed because the siloxane-based column does not provide enough retention for low molecular weight amines.²³

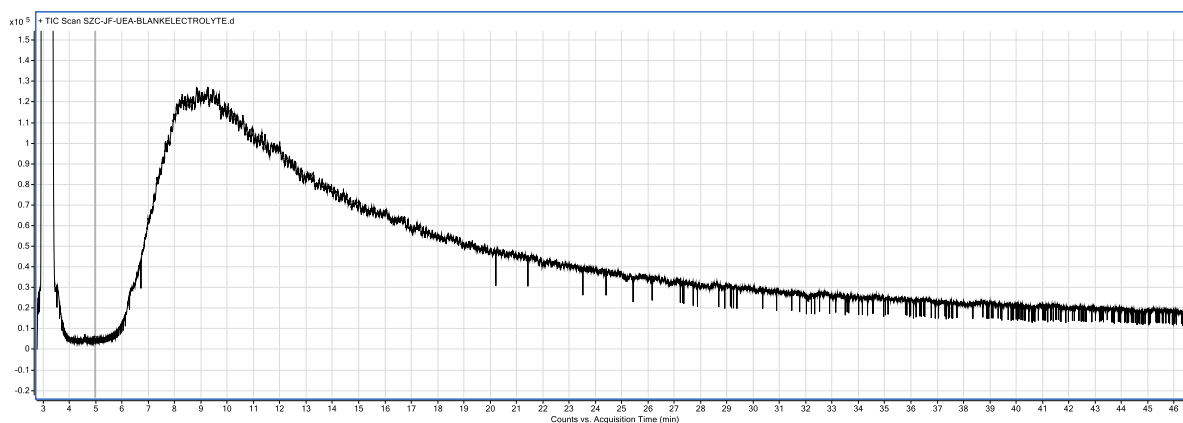


Figure S28. GC trace of unreacted 0.1 M NBu_4BF_4 electrolyte, showing the absence of any of the products identified from the bulk electrolysis catholyte.

References

1. W. L. F. Armarego and C. L. L. Chai, *Purification of laboratory chemicals*; 6th ed.; Elsevier/Butterworth-Heinemann: Amsterdam; Boston, 2009.
2. J. Fielden, J. Sprott and L. Cronin, *New J. Chem.* 2005, 1152.
3. (a) G. Kallinger and R. Neissner, *Mikrochim. Acta* 1999, **130**, 309. (b) F. Sacher, S. Lenz and H.-J. Brauch, *J. Chromatogr. A* 1997, **764**, 85.
4. Clarity Version 3.06.589, Data Apex Ltd, Prague, Czech Republic, 2011.
5. J. T. Groves and M. Van Der Puy, *J. Am. Chem. Soc.* 1976, **98**, 5290.
6. B. Elchert, L. Jie, J. Wang, Y. Hui, R. Rai, R. Ptak, P. Ward, J. Y. Takemoto, M. Bensaci, and C.-W. T. Chang, *J. Org. Chem.* 2004, **69**, 1513.
7. S. K. Ibrahim, Ph.D Thesis, University of Sussex, 1992.
8. *CrysAlisPro* (Version 1.171.36.21), Agilent Technologies, Inc.; Santa Clara: CA, United States, 2012.
9. *CrysAlisPro* Software System, Rigaku Oxford Diffraction, Yarnton, Oxford, UK, 2015.
10. G. M. Sheldrick, *Acta Cryst.* 2015, **A71**, 3–8.
11. O. V. Dolomanov, L. J. Bourhis, R. J. Gildea, J. A. K. Howard and H. Puschmann, *J. Appl. Cryst.* 2009, **42**, 339.
12. G. M. Sheldrick, *SHELXS-2014*, Programs for Crystal Structure Analysis (Release 2014-7); University of Göttingen: Göttingen, Germany, 2014.
13. L. J. Farrugia, *J. Appl. Cryst.* 1999, **32**, 837.
14. G. M. Sheldrick *SHELXL-2014*, Programs for Crystal Structure Analysis (Release 2014-7); University of Göttingen: Göttingen, Germany, 2014.
15. L. J. Farrugia, *J. Appl. Cryst.* 1997, **30**, 565.
16. CCDC, *Mercury 3.8*, Cambridge Crystallographic Data Centre, Cambridge, UK, 2016.
17. J. Fielden, D.-L. Long, M. Speldrich, P. Kögerler and L. Cronin, *Dalton Trans.* 2012, **41**, 4927.
18. M. J. Frisch, G. W. Trucks, H. B. Schlegel, et al.; Gaussian 09, Revision B.01 *Gaussian 09, Revision B.01*, Gaussian, Inc., Wallingford CT. 2009.
19. C. Adamo and V. Barone, *J. Chem. Phys.* 1999, **110**, 6158.
20. J. Ho and M. Z. Ertem, *J. Phys. Chem. B* 2016, **120**, 1319.

21. P. J. Hay and W. R. Wadht, *J. Chem. Phys.* 1985, **1**, 270.
22. G. R. Salazar-Banda, A. E. de Carvalho, L. S. Andrade, R. C. Rocha-Filho, L. A. Avaca, *J. Appl. Electrochem.*, 2010, **40**, 1817.
23. Agilent Technologies, Inc, *Amines, C₁ – C₂, Analysis of impurities in dimethylamine*, Application Note A01398, 2011.